

<b>Project</b>	H2020 - SURE (Grant-Number 654662)
<b>Deliverable</b>	D7.4 - Upscaling of RJD for incorporation in reservoir simulators
<b>Work package</b>	WP7 - Integration
<b>Lead authors</b>	Elisabeth Peters and Paul Egberts (TNO)
<b>Contributor(s)</b>	Alin Chitu and Rohith Nair (TNO), Saeed Salimzadeh (DTU), Guido Blöcher and Mauro Cacace (GFZ)
<b>Dissemination level</b>	PU (public)
<b>Type</b>	R (document, report)
<b>Due date</b>	30 November 2018
<b>Actual submission date</b>	30 November 2018
<b>Change History</b>	08 June 2020 - Licence, DOI and Citation Information added

<b>Licence information</b>	Report D7.1 of the Consortium of the H2020 SURE Project This publication is licensed under a Creative Commons License, International Attribution 4.0: CC BY
<b>DOI (Repository)</b>	10.2312/gfz.4.8.2019.003
<b>Recommended Citation</b>	E. Peters, P. Egberts, A. Chitu, R. Nair, S. Salimzadeh, G. Blöcher, M. Cacace.; The Horizon 2020 Project SURE: Deliverable 7.4 - Upscaling of RJD for incorporation in reservoir simulators 2018, Potsdam: GFZ German Research Centre for Geosciences, DOI: <a href="https://doi.org/10.2312/GFZ.4.8.2019.003">https://doi.org/10.2312/GFZ.4.8.2019.003</a>

## Table of Contents

<b>1</b>	<b>Executive Summary .....</b>	<b>3</b>
<b>2</b>	<b>Introduction .....</b>	<b>4</b>
<b>3</b>	<b>State-of-the-art in upscaling of well inflow modelling.....</b>	<b>6</b>
<b>4</b>	<b>Implementation of well inflow modelling.....</b>	<b>11</b>
<b>5</b>	<b>Comparison of RJD well modelling .....</b>	<b>14</b>
<b>6</b>	<b>Well testing .....</b>	<b>15</b>
6.1	Radius of influence .....	15
6.2	Transient solution.....	17
6.2.1	Wellbore storage.....	18
6.3	Results.....	19
6.3.1	Radial well base case.....	19
6.3.2	Validation .....	20
6.3.3	Well test type curves for radial wells .....	21
<b>7</b>	<b>Summary and conclusions.....</b>	<b>25</b>
	<b>Acknowledgements.....</b>	<b>25</b>
	<b>Nomenclature.....</b>	<b>26</b>
	<b>Table of Figures.....</b>	<b>26</b>
	<b>Table of Tables .....</b>	<b>27</b>
	<b>References .....</b>	<b>27</b>
	<b>Appendix A. Evaluation of WI amalgamation options.....</b>	<b>30</b>
	<b>Appendix B. Running and testing of the WIC tool.....</b>	<b>33</b>
	<b>Appendix C. Eclipse model used for simulating well testing.....</b>	<b>39</b>
	<b>Appendix D. Peters et al. (2018) Modelling of multi-lateral well geometries for geothermal applications. Advances in Geosciences, 45: 209-215. ....</b>	<b>41</b>

## 1 Executive Summary

To economically produce a geothermal resource, wells with sufficient productivity or injectivity are a key element. However, for a variety of reasons well productivity can be lower than expected or decline over time, for example because of disappointing reservoir transmissivity or because of well problems, such as scaling or near well bore damage. One of the options to enhance the productivity or injectivity of a well is Radial Jet Drilling (RJD). With this technology, laterals of up to 100 meters length and with a diameter of around 1" (inch) can be hydraulically jetted from the main well bore. This technique has been developed in the petroleum industry but is relatively new for geothermal applications.

Prediction of the performance of well configurations obtained from RJD is imperative in the design phase of a radial well. For robust planning and optimization of a radial well design, numerous simulations for many reservoir models and well configurations are required. To achieve this, in this study first an efficient numerical simulation method for radial wells is selected and validated. Next, the method is automated in a software tool for application in sensitivity analysis and optimization workflows.

Several numerical methods exist that potentially can be used for the simulation of radial wells. A complication of modeling well inflow (or outflow) using numerical methods is the large difference in dimensions of a well diameter and grid block sizes. To increase the efficiency of the simulation, an upscaling approach is often used that allows usage of relatively large grid blocks, compared to the well's diameter, which is the well index concept. In this concept, the well is not simulated explicitly but incorporated as a sink. The pressure drop between the (large) grid block in which the well is located and the well is calculated based on the geometry of the well and the properties of the grid block. This widely used concept is further analyzed for radial well configurations in combination with a Finite Volume reservoir simulator (Eclipse®).

To validate the well index concept, a comparison was made between three numerical simulators and a semi-analytic approach. The distinct approaches are the Finite Element Method with the well modeled explicitly by elements, the Finite Volume Method using the upscaling concept of well indices and the Analytic Element Method. It was found that simulators are mutually close with regard to the total flow rate but may differ considerably in how well inflow is distributed over the well segments (backbone and laterals). This study confirmed the accuracy and efficiency of the FV approach with well index concept.

The next step is the automation of the well index calculation in a stand-alone software tool. The calculation of the well index is supported in some commercial tools, but these are not suitable for incorporation in automated workflows. Therefore a tool was developed that calculates the well indices and grid block indices needed by the FV simulator. The calculation is based on a geometrical description of the radial well, the grid definition and grid properties such as permeabilities.

Besides using mathematical models for well performance prediction during the design phase, modelling may also assist in estimating well and reservoir characteristics after the implementation of the well in the field through interpretation of pressure transient data obtained from well tests. For that, the inhouse AEM tool was extended to derive the full pressure transient solution for a radial well including wellbore storage effects. A strength of the followed approach is that the geometry of the laterals is explicitly accounted for in contrast to standard approaches using a vertical or deviated well with a (negative) skin to incorporate well stimulation effects. Including the well geometry potentially allows to

estimate the effectiveness of the jetting of the laterals, in particular the lateral reach may be highly uncertain. The semi-analytic approach was successfully validated with a numerical model with a very fine grid allowing to represent the well explicitly. As demonstration of the developed method several pressure and pressure derivative type curves for well test interpretation are shown.

## 2 Introduction

To economically produce a geothermal resource, wells with sufficient productivity or injectivity are a key element. However, for a variety of reasons well productivity can be lower than expected or decline over time, for example because of disappointing reservoir transmissivity or because of well problems, such as scaling or near well bore damage. One of the options to enhance the productivity of a well are small-diameter laterals. For bypassing a skin such a lateral need not be very long (up to 10 m should be enough), but for connecting the reservoir better to the well in case of e.g. low permeability, longer laterals are needed. A technique which can achieve a distance of up to 100 m is radial jet drilling (RJD). This technique has been developed in the petroleum industry but is relatively new for geothermal applications. With the technology, laterals of up to 100 meters length and with a diameter of around 1" (inch) can be hydraulically jetted from the main well bore (Figure 2-1).

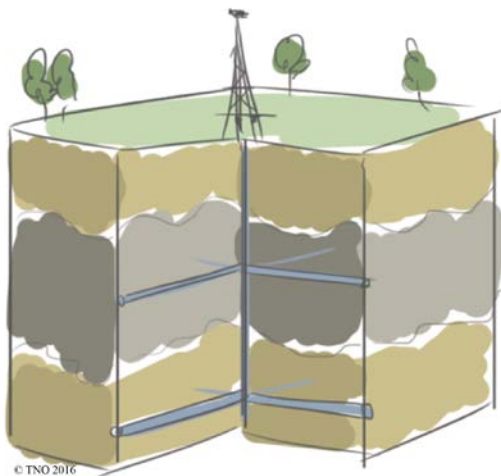


*Figure 2-1. Overview of well geometry created using radial jet drilling.*

Simulation of liquid flow from or into a well with a geometry created using RJD is important for planning of a radial jet drilling job and prediction of the production or injection performance after implementing the laterals. Such a well, referred to as a radial well, is a complex well with multiple laterals (sometimes called radials in this report) that may have the same kickoff location at the backbone. The diameters of the backbone and radials differs in magnitude with smaller diameter for the jetted radials. The complex well configuration poses difficulties to model the inflow into the well and its laterals accurately, especially when using an irregular grid, such as those used to represent realistic geological conditions [41]. Furthermore, it can be challenging in numerical simulation to correctly account for interference between the well segments. One of the goals of the presented work is to investigate what method(s) provide efficient and accurate simulations for radial wells on field scale.

Common fluid flow simulators for geothermal applications ([23], [39]) are TOUGH2 [29], Eclipse® [34], STARS [37] which are based on the Finite Volume (FV) method, TETRAD and SHEMAT [35] are based on the Finite Difference method (FD) and, using Finite Element approaches (FE), Feflow® [12], GOLEM [6], CSMP (combined FEFV method) [6] and PANDAS [24]. Although many different numerical approaches are used, the challenges for well inflow modelling on reservoir scale are similar: a huge difference in the dimensions of a well and the reservoir. Typically, a well has a diameter in the order of 0.1 m while a reservoir may have a surface area as large as 100 km<sup>2</sup>. Theoretically one may opt for small grid blocks near the well to model the well explicitly. This, however, will lead to large numbers of grid blocks and increased simulation times, especially in the case of multiple wells. Also, too coarse grids will quickly lead to wrong simulated flow rate and/or pressure drop.

To solve the problem of many, small grid blocks, an upscaling step is required. We have selected the concept of the well index (or well connection factor), which is a transmissibility factor for calculating well inflow, as the most suitable method for upscaling. The well index concept as implemented in FD or FV approaches will be explained in Chapter 3. Implementation of the well index for Finite Element methods is not discussed.

To find a robust radial well design by hand may be too cumbersome due to the large number of design parameters and possibly large number of reservoir models needed for uncertainty assessment. Therefore, automated workflows for sensitivity analysis and optimization are developed and applied in Tasks 7.5 and 7.6. Using a reservoir simulator exploiting the well index upscaling concept in these workflows requires repeatedly the calculation of the well indices to be used by the simulator. Commercial tools with functionality to calculate well indices are available ([28]) but are not useable in iterative and automated workflows required for sensitivity analysis and optimization. Therefore, a dedicated tool was developed to calculate inflow parameters, in particular well indices, from the well geometry, the numerical grid and the gridded reservoir properties. This is described in Chapter 4.

In Chapter 5, the results of the well index approach are compared to results of other simulation approaches among which a semi-analytical approach. This is the closest we can get to validation of the approach, since no observed data is available which is sufficiently accurate for validation. Also, given the fact that radials cannot be logged, such a data set is not expected. Flow measurements from radial wells are available, but no observations of radial paths. The uncertainty in the simulation results due to uncertainty in the radial path is larger than the uncertainty because of the use of the well index.

The concept of the well index is useable in numerical reservoir simulators, but not in the tools commonly used for well test analysis, which generally rely on analytical solutions [18]. Currently the only option for interpreting a well test of a radial well is to interpret the radials as a negative skin. In Chapter 7, we present a semi-analytical tool which can accurately simulate the transient behaviour of a multi-lateral or radial well. This tool can be used to properly interpret well tests for radial wells.

### 3 State-of-the-art in upscaling of well inflow modelling

In many numerical reservoir simulations, the dimension of a well with well radius  $\sim 0.1$  m is much smaller than the grid block size, which can have a lateral extend of the order of 10-100 m. To deal with these different scales the Well Index (WI) concept is used to couple well inflow with grid block quantities such as grid block pressure and permeability. The well index can be seen as a transmissibility factor relating the difference of the grid block pressure and the well pressure to the well inflow in case of production (or outflow in case of injection).

Although the well index concept is very useful for upscaling the well modelling, some detailed aspects of flow cannot be accounted for. The most important limitation is that the location of the well inside the grid blocks is not accounted for. It is assumed that the well is always in the centre of a grid block [10]. The errors resulting from this approximation can be mitigated by placing the well in the middle of grid blocks whenever possible, or by using sufficiently fine grids. What sufficiently fine is, is difficult to define up front. Simulation with increasingly fine grids should be used to verify the accuracy of the solution. For radials of 100 m length, it was found the grid blocks of 10 to 20 m are usually sufficiently small.

Also not accounted for in the WI calculation are:

- Detailed near-well processes such as preferential flow paths.
- Accurate pressure losses due to non-linear effects (Forcheimer) which depend on velocity. These effects can only be included averaged over the grid block or as a non-linear, rate dependent skin for a well. This is mainly important in case of steam.
- Velocity in a fracture.
- Detailed effects of cooling, especially in preferential flow paths such as fractures or high-perm streaks due to the assumption of constant properties within a grid block.
- Thermal diffusion

In a FV or FD approach a well is discretised in a number of well connections (well nodes) with each connection associated to a grid block intersected by the well. We will call a grid block intersected by the well a well block and the intersection a well segment.

The well index  $WI_i$ , of well segment labeled by index  $i$ , is defined by, see e.g. [41]:

$$q_i = \frac{WI_i}{\mu} (p_{b,i} - p_{w,i}) \quad (1)$$

with  $\mu$  the viscosity. The well index relates the difference of well pressure  $p_{w,i}$  and well block pressure  $p_{b,i}$  to the flow rate  $q_i$  of segment  $i$ .

Instead of well index also the terms well connectivity factor or connection transmissibility factor are used. The Well Index should not be confused with the Productivity Index (PI) and/or Injectivity Index (II) relating flow rate of the entire well to pressure drawdown in the reservoir.

The definition and use of  $WI$  as such is straightforward. The difficulty lies in determining an accurate value for  $WI$ . Different simulators use different approaches. For TOUGH2,  $WI$  is to be provided separately by the user and according to the manual can be calculated, assuming steady state flow, as follows [29], [42], [5]:

$$WI_i = \frac{2\pi(kh)_i}{\ln(r_{e,i}/r_{w,i}) + S_i - \frac{1}{2}}$$

Where,

- $kh$  : product of permeability and length of the well segment
- $r_e$  : radius of circle with same area as well block
- $r_w$  : well radius
- $S$  : skin factor

The subscript  $i$  of the above quantities is to indicate their dependency on the location of the well segment in the grid. For notational convenience we will omit the subscript from here on. For pseudo-steady state flow, the correction factor  $-1/2$  can be replaced by  $-3/4$ . For cylindrical well blocks,  $r_e$  is equal to the radius of the well block. For cartesian grids,  $r_e$  can be calculated as:

$$r_e = \sqrt{\Delta x \Delta y / \pi}, \quad (2)$$

where  $\Delta x \Delta y$  is the area of the well block.

In the  $WI$  formulation above single phase is assumed which is appropriate for our application. We suffice with noting that the  $WI$  concept can be naturally extended to multiphase flow, see e.g. [3]

In the petroleum industry, well index calculations are usually based on the work by Peaceman [25], [26]. Peaceman showed in [25] that Eq. (2) implicitly assumes that the numerically calculated well block pressure is equal to the areal averaged pressure. He showed that this assumption is not correct and defines an *equivalent well block radius*  $r_{eq}$  as the radius at which the analytical radial flow pressure equation equals the well block pressure which gives a different interpretation of the well block pressure.  $WI$  then becomes, based on the new well block pressure interpretation:

$$WI = \frac{2\pi kh}{\ln\left(\frac{r_{eq}}{r_w}\right) + S} \quad (3)$$

For square gridblocks in an isotropic medium,  $r_{eq}$  was found to be:

$$r_{eq} \approx 0.2\Delta x \quad (4)$$

The concept of equivalent well block radius was extended by Peaceman in [26] for non-square gridblocks in an anisotropic medium. For a vertical well,  $WI$  is given by (3) with equivalent well block radius given by

$$r_{eq} = 0.28 \frac{\sqrt{\left[ \sqrt{\frac{k_y}{k_x} \Delta x^2 + \frac{k_x}{k_y} \Delta y^2} \right]}}{\left[ \sqrt[4]{\frac{k_y}{k_x}} + \sqrt[4]{\frac{k_x}{k_y}} \right]} \quad (5)$$

and permeability thickness term  $kh$  replaced by  $\sqrt{k_y k_z} h$ .

Especially for small grid blocks, the difference between the TOUGH2 and Peaceman approach becomes large (Figure 3-1).

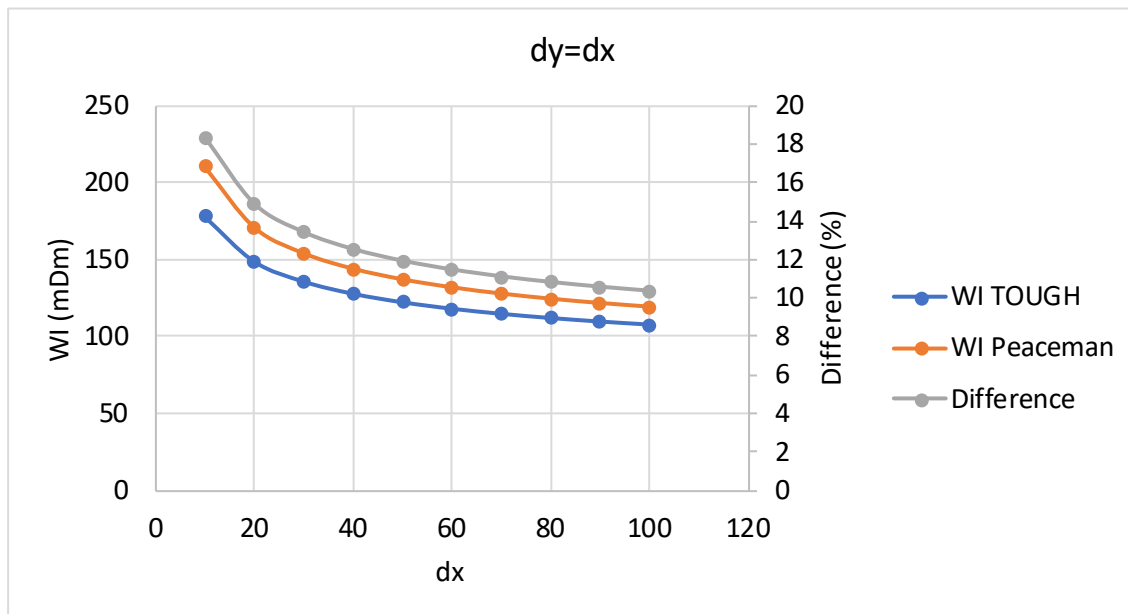


Figure 3-1. WI calculated using the approach as described in TOUGH2 manual ([5], [29]) and following Peaceman.

In the derivation of  $r_{eq}$  Peaceman assumed that the well is centred, aligned to a grid axis, isolated from other well segments so that radial flow near the well is implied. Generally these assumptions are to some extent violated for the radial well configurations considered in this work. Thus for cartesian grids with aligned wells, equations (3) and (5) provide accurate results, but may be inaccurate for unconventional wells such as multi-lateral wells or radial wells in geologically complex grids. In particular an trajectory of unconventional well in a geologically based numerical grid will generally not be aligned to permeability grid axis. This may lead to erratic inflow [10]. Different schemes have been proposed for improved definitions of permeability-thickness  $kh$  and equivalent well block radius  $r_{eq}$  that do not assume that the well is aligned with the grid and/or that only one segment intersects with a single grid block:

- Scaled WI: Two main methods proposed are by Alvestad et al. [2] and the projection technique by Holmes [33]. Both methods have been compared in [1] and in [36].
- Semi-analytical approaches: The use of semi-analytic well indices have been studied by several authors ([1], [10], [41]). Wolfsteiner et al. [41] developed a general procedure to calculate semi-analytic well indices for complex wells and arbitrary grids using a semi-analytic well model.

In [10] a combination of a semi-analytical reservoir model based on the Analytic Element Method ([9], [15]) and a dedicated reservoir simulation model to arrive at the semi-analytic well indices. It was demonstrated that using semi-analytic well indices certain numerical artefacts can be removed.

In practice, the semi-analytical approaches are rarely used because they are generally quite complex to apply. The scaled approaches are easy to implement and will be discussed in the following. The projection method or three-part Peaceman formula is implemented in Petrel® [33]. The well intersection is calculated by projecting the well intersection of a grid block on three locally defined orthogonal axes interpreted as the direction of the permeabilities  $k_x$ ,  $k_y$  and  $k_z$  and calculating  $WI$  for each of those projections. In case of an orthogonal grid the local orthogonal axes coincide with the grid axes (Figure 3-2).

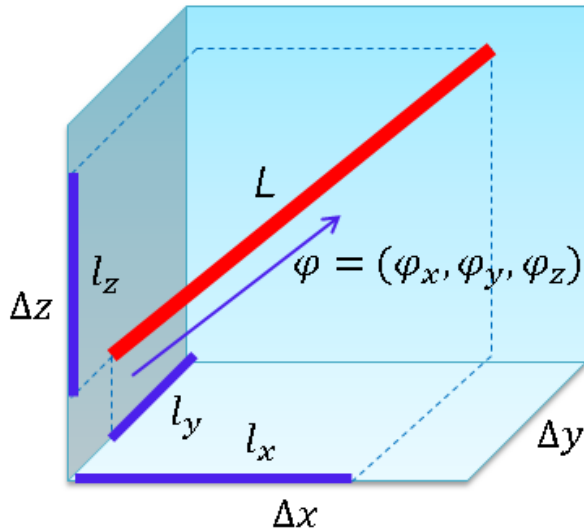


Figure 3-2. Illustration of the projection approach. Red line is the well segment in the well block, the three blue lines are the projections on the permeability axis.

The well index  $WI_x$  for the projected well segment aligned to the  $x$ -axis becomes

$$WI_x = \frac{2\pi\sqrt{k_y k_z} l_x}{\ln\left(\frac{r_{eq,x}}{r_w}\right) + S} \quad (6)$$

with

$$r_{eq,x} = 0.28 \frac{\sqrt{\left[ \sqrt{\frac{k_y}{k_z}} \Delta z^2 + \sqrt{\frac{k_z}{k_y}} \Delta y^2 \right]}}{\left[ \sqrt[4]{\frac{k_y}{k_z}} + \sqrt[4]{\frac{k_z}{k_y}} \right]}$$

Similarly,  $WI_y$  and  $WI_z$  can be derived. The well index  $WI$  for the well segment is defined by

$$WI = \sqrt{WI_x^2 + WI_y^2 + WI_z^2} \quad (7)$$

Note that if the well segment is aligned to the one of the axis,  $WI$  reduces to the standard Peaceman well index. The Petrel method computes the well index from individual

Version 6/8/2020	Upscaling of RJD for incorporation in reservoir simulators	page 10 / 41
------------------	--	--------------

contributions  $WI_x$ ,  $WI_y$  and  $WI_z$  where the contribution from multiple segments within a single grid block can be taken into account (See e.g. [36]).

A second possible correction is due to Alvestad [2], [10]. Assuming that the well intersection with a gridblock  $i$  is linear then the permeability-thickness product is given by

$$kh_i = \sqrt{k_x k_y l_z^2 + k_x k_z l_y^2 + k_y k_z l_x^2},$$

where  $(l_x, l_y, l_z)^T$  is the direction vector denoting the well path increment of the well in the grid block (Figure 3-2). For the calculation of  $r_{eq}$  the Alvestad's method uses [2]:

$$r_{eq} = G \frac{\sqrt{L_1^2 + L_2^2}}{\sqrt{A_1 + A_2}},$$

where

$$L_1^2 = \Delta z^2 \psi_x^2 \sqrt{\frac{k_y}{k_z}} + \Delta x^2 \psi_y^2 \sqrt{\frac{k_z}{k_x}} + \Delta y^2 \psi_z^2 \sqrt{\frac{k_x}{k_y}},$$

$$L_2^2 = \Delta y^2 \psi_x^2 \sqrt{\frac{k_z}{k_y}} + \Delta z^2 \psi_y^2 \sqrt{\frac{k_x}{k_z}} + \Delta x^2 \psi_z^2 \sqrt{\frac{k_y}{k_x}},$$

and

$$A_1 = \psi_x^2 \sqrt{\frac{k_y}{k_z}} + \psi_y^2 \sqrt{\frac{k_z}{k_x}} + \psi_z^2 \sqrt{\frac{k_x}{k_y}}, \quad A_2 = \psi_x^2 \sqrt{\frac{k_z}{k_y}} + \psi_y^2 \sqrt{\frac{k_x}{k_z}} + \psi_z^2 \sqrt{\frac{k_y}{k_x}},$$

here,  $\Delta x$ ,  $\Delta y$  and  $\Delta z$  are the gridblock dimensions, and  $\psi_x$ ,  $\psi_y$  and  $\psi_z$  are the components of the normalized direction vector  $\psi$  of the well segment in the grid block,  $G = \frac{1}{2}e^{-\gamma} \approx 0.2807298$ , with  $\gamma$  the Euler constant. Alvestad's formula reduces to the Peaceman's formula when the directional vector  $\psi$  is aligned with the one of the grid block axes.

Aavatsmark et al. [1] note that the two methods do not produce identical results. They refer to the projection method as the 'SCHEDULE' method and refer to the Petrel user guide for building the schedule section for Eclipse.

### Fractured media

Up to this point only well inflow in porous media has been discussed. However, in many geothermal reservoirs fractures have a large impact on the inflow behaviour of the well, either by natural fracture networks or induced fractures in EGS [4]. Different model approaches are available, which can broadly be divided in two groups

- Approaches that assume a statistical distribution of fractures in which the flow can effectively be described by Darcy's law. These are called dual continuum models, which can be subdivided in *dual porosity* and *dual permeability* models [17]. In a *dual porosity* medium, the flow in the reservoir and into the well is through the fracture network. There is flow from matrix to fractures but negligible flow through the matrix system i.e. matrix act as a fluid storage. In a *dual porosity-dual permeability* medium, flow in the reservoir and into the [17] well occurs both via fractures and matrix. Flow in the matrix occurs over longer distances in contrast to a dual porosity system.

- Discrete fracture network (DFN) approaches in which the flow in fractures is simulated explicitly [7]. This is generally done when the flow into the well is dominated by individual fractures. This allows incorporation of more detailed processes such as non-Darcy flow in the fractures and heterogeneity of fracture aperture and the impact on cooling [17].

For dual porosity and/or dual permeability media, the well inflow modelling is essentially the same as for single porosity media. For dual porosity media the same WI formulations can be used as described in the previous section except that the permeability should be taken as the bulk permeability (effective permeability) of the dual porosity media.

In case of *dual porosity-dual permeability* medium, two WI's per well segment are identified: one for fracture system, one for matrix system. The WI for the fracture uses the pressure in the fracture system and for the matrix the matrix pressure is used. Application of the well index concept in DFN approaches is not discussed here, because the concept is not appropriate. The well index concept can however be applied to the matrix flow part of a DFN simulation [32].

If these processes are important in a particular case, a different, more detailed approach is required. This is not further discussed in this report.

#### 4 Implementation of well inflow modelling

In this chapter a description is presented of the implementation of well index calculations, described in Chapter 3, in a dedicated software tool applicable for radial well configurations. A standalone software tool for the calculation of the well index enables efficient workflows for sensitivity analysis and mathematical optimization for radial wells.

Sensitivity analysis or, more involved, mathematical optimization is required to systematically evaluate what the “best” design is considering uncertainty, well costs and technical limits. These approaches will be discussed in Tasks 7.5 and 7.6. Numerous reservoir simulations need to be performed in a systematic and automated way. This requires iterative workflows that can be run in batch mode to manage the reservoir simulations, in this case Eclipse. This excludes the usage of an application like Petrel that requires input via a GUI and is commonly used by reservoir engineers to define wells in the numerical reservoir model. Having defined a well, Petrel generates the relevant well data required by Eclipse to execute a reservoir simulation.

The needed flexibility for automation of workflows prompted the development of a tool that can calculate, in batch, the well data needed by Eclipse (and thus circumventing Petrel involvement). This tool basically combines grid properties such as permeabilities and grid sizes and the radial well geometry to calculate the well block indices and associated well indices. How the well indices are calculated, including for well blocks containing multiple well segments, has been elaborated in the previous chapter. Only for the calculation of the well index at the connection point of the laterals with the backbone, no solution could be found in literature and this is discussed below.

##### *WI at the connection of laterals and backbone*

The well index calculation gives a problem for radial wells due to the common occurrence of multiple well segments in a single grid block, where the segments from the laterals have a different diameter than the backbone. Because of the difference in diameter and orientation, it

Version 6/8/2020	Upscaling of RJD for incorporation in reservoir simulators	page 12 / 41
------------------	--	--------------

is not straightforward to calculate a representative  $WI$  for the single wellblock. It is not clear how Alvestad's formula can be generalized for the case that there are multiple segments within a single grid block since it is based on a single normalized direction vector (see [10]). Therefore, the projection approach is used to solve this problem.

To keep notation simple, assume two well segments (e.g. one backbone and one lateral segment) in a single cell with respective well indices  $WI_1$  and  $WI_2$  where  $WI$  is calculated using the projection approach:

$$WI_i = \sqrt{WI_{i,x}^2 + WI_{i,y}^2 + WI_{i,z}^2}, \quad i = 1,2$$

There are several choices to arrive at a total well index  $WI_{t,i}$ :

$$A. WI_t^A = WI_1 + WI_2 = \sqrt{WI_{1,x}^2 + WI_{1,y}^2 + WI_{1,z}^2} + \sqrt{WI_{2,x}^2 + WI_{2,y}^2 + WI_{2,z}^2}$$

$$B. WI_t^B = \sqrt{(WI_{1,x} + WI_{2,x})^2 + (WI_{1,y} + WI_{2,y})^2 + (WI_{1,z} + WI_{2,z})^2}$$

$$C. WI_t^C = \max(WI_1, WI_2).$$

In option A it is assumed that there is no interference between the two well segments and it thus represents an upper bound; any well index formulation should provide a value less or equal to  $WI_t^A$ . In option B an effective length for the well is calculated by summing the x, y and z-components first. This assumes interference between the two well segments and gives lower estimates for the WI than option A. The lower bound of WI would be the WI of the largest element, that is option C assuming total interference (no contribution of the smaller WI). The actual amount of interference depends on the configuration of the well, permeability and the grid size. Summarizing, we have the following ordering  $WI_t^C \leq WI_t^B \leq WI_t^A$ .

To choose which option to use, options A, B and C can be calculated for different well configurations and compared to the results of a semi-analytical solution of the same well configuration (see Chapter 5 and Appendix D for a description of the semi-analytical method). This has been done for a vertical well with 4 laterals of 50 and 20 m in a grid of 20 x 20 x 5 m (see Appendix A for details). The results showed that the difference in flow rate between options A, B and C is smaller than the error in the flow rate calculation due to the numerical discretization. This is due to two aspects:

- For fine grids (compared to the well length), numerical errors are small (< 4%, see next chapter), but the impact of option A, B or C is also small (< 1% in Appendix A).
- For coarse grids, the impact of option A, B or C is larger, but so is the numerical error of the simulation of the flow rate (see Appendix A).

In conclusion, the impact of the calculation method of the WI for the case with multiple segments cannot be resolved from numerical simulation. Therefore we decided to use method B for our project, firstly because it can be applied in all cases, secondly because it is in line with the definition of WI for a single, non-aligned segment in Eq. (7) and thirdly because it is known that flow interference between well segments occurs [27]. The choice of this method is not further discussed in the RJD well modelling comparison in the next chapter.

Detailed results can be found in Appendix A.

*Implementation*

The well index calculation is implemented in a tool, which is referred to here as the WIC (Well Index Calculation) tool. The tool combines the grid properties contained in Eclipse files \*.EGRID (or \*.grid) and \*.INIT (permeabilities and grid size) with the well path to produce the COMPDAT section that is part of the Eclipse input specification (Figure 4-1). The COMPDAT section specifies the well location in terms of well block indices and all parameters needed for the calculation of well inflow.

Starting point of the tool development is the open source code FieldOpt from NTNU [13]. In collaboration with NTNU, this code has been extended further to allow for well indices calculation for multilateral wells. The most important step for the calculation of the WI is the calculation of the intersection of the well with the grid, which results in a list of the grid blocks intersected by the well and the length of the intersections. The search for the well blocks is the most time-consuming part of the calculation. The following steps are taken:

- Calculate the points where the well intersects the grid block faces. The two intersection points determine the well intersection inside the grid block  $\vec{w}$ .
- Determine local  $x$ ,  $y$  and  $z$  directions based on the grid block corner points (assuming planar grid block faces). These directions are not necessarily orthogonal.
- Project the well length in the grid cell onto the local  $x$ ,  $y$  and  $z$  directions: that results in the lengths  $l_x$ ,  $l_y$  and  $l_z$  according to (Euclidian norm):

$$l_x = \left\| \vec{x} \frac{\vec{x} \cdot \vec{w}}{\vec{x} \cdot \vec{x}} \right\|$$

This way of calculating the well length for the  $x$ ,  $y$  and  $z$  direction is different from the implementation in Petrel and thus the calculation WI will differ from the results in Petrel (see ‘connection factor calculation’ in [33]) but is in full agreement for simple orthogonal grids. The difference is especially noticeable in deviated wells in tilted grids.

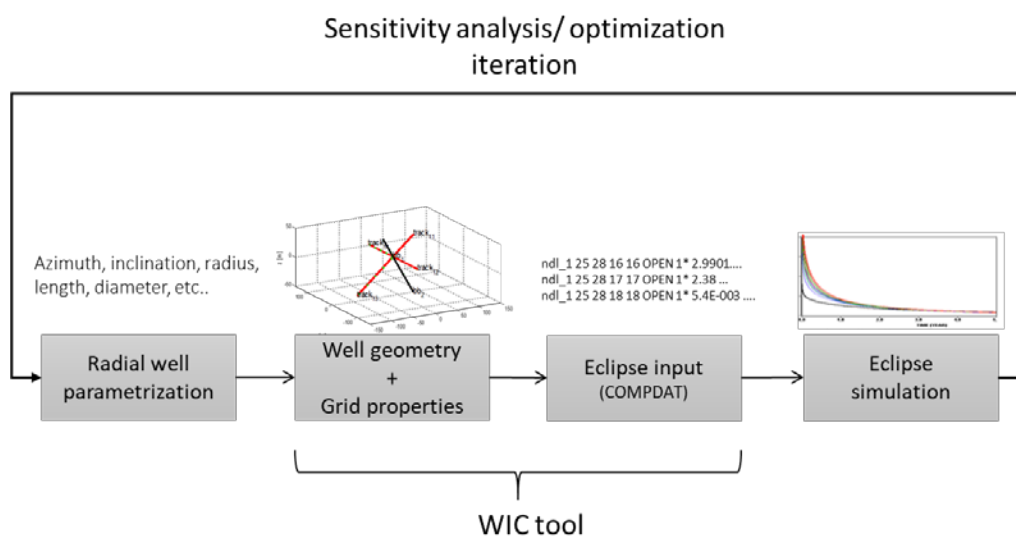


Figure 4-1. From parametrization to reservoir simulation.

The following changes were made to the original NTNU code:

- The original code could handle only a single segment. The updated code can handle multiple linear segments within one well and multiple wells.

- The updated code can handle both single and dual porosity grids.
- A skin can be defined per well segment.
- Improvements were made to find the intersection of the well with grid faces in various situations.
- The original code could handle only one definition of the orientation of the grid. However, Eclipse grids can come in several definitions, which can be indicated by the grid axis. The updated code has been made more flexible in handling these definitions.
- Calculation of the intersection of the grid block faces with the well has been speeded up.

Appendix B gives more details on how to run the WIC tool and the results of tests done to check the implementation of the tool.

## 5 Comparison of RJD well modelling

Validation of a model approach is preferably done using observed data of the simulated properties. This requires both input and output to be observed with a high accuracy. For a radial well, no data set is available which is sufficiently detailed and accurate. Also, considering the limited monitoring options for radials (e.g. no logging of the radial), such a data set is not likely to become available soon. Also a validation of the well index approach using other numerical methods is impossible, because all numerical approaches have inaccuracies. However, a comparison of different methods can reveal inaccuracies when the results are different. In [28] (reproduced in Appendix D) a comparison of calculating inflow into a radial well is presented with four different approaches: three numerical simulators and a semi-analytical tool. The numerical simulators are two FE approaches (CSMP and GOLEM) in which the well is simulated explicitly and an FV approach with a well model (Eclipse®). The semi-analytical tool is based on the Analytical Element Method (AEM). In this method a pressure solution can be derived, for a homogeneous reservoir, satisfying predefined flow and pressure boundary conditions at the well and reservoir. The solution takes fully into account the 3D character of the flow around the well. A series of increasingly complex well configurations is simulated, including a case with inflow from a fault. The first two cases which are simulated have homogeneous reservoir properties, because these can be simulated by the semi-analytical tool. In the third case, laterals are used to connect to a fault. The laterals are approximated by straight well segments although it is unlikely that they are straight in the subsurface [29].

Although all simulators generally are mutually close in terms of the total well flow (deviations < 4 % for the homogeneous cases), the distribution of the flow over the different parts of the well can vary up to 20 % for some laterals. For the homogeneous cases (1 and 2 in [28]), the predictions of increase of flow as a result of stimulation by RJD show a range of variation up to 5 % just from differences between numerical solutions even for a simple setup. In realistic implementations with heterogeneous reservoir properties, larger uncertainty from the numerical solution can be expected for all simulators: for Eclipse because of inaccuracies in the calculation of the well index and for the FE approaches because of difficulties in determining the correct mesh size and large number of elements. In case the flow is dominated by fracture flow, the results deviate more with up to 50 % difference in the predicted flow rate in the case of radials. Even though these uncertainties are considerably smaller than those arising from uncertainty in the properties and uncertainty in the radial path, it is a source of errors that is often ignored.

Version 6/8/2020	Upscaling of RJD for incorporation in reservoir simulators	page 15 / 41
------------------	--	--------------

## 6 Well testing

For most well tests a controllable surface injection or production rate is changed and the pressure response in the well is measured. Through matching the pressure response with a mathematical (semi-analytical or numerical) model, certain reservoir and well parameters may be estimated [18]. Examples of such parameters are reservoir permeability, skin factor, reservoir dimensions and fracture characteristics in case of a naturally fractured reservoir. Matching well test result, requires a model that captures transient behaviour. To our knowledge, semi-analytic models used in well test software are not capable of incorporating explicitly the complex radial well geometry. This limits the possibility to estimate radial well characteristics and thus to test the effectiveness of the jetting of the radials.

The explicit modelling of the well configuration rather than expressing the stimulation by representing radials through a (negative) skin factor, potentially allows to retrieve from well test data, estimates of the well configuration such as the extend of radials. Furthermore, lumping the additional gain of the jetted radials into a skin factor is too coarse for describing early pressure transients as the extend of the radial is typically in the order of 10-100 m.

To enable well testing of radial wells, the inhouse AEM (Analytical Element Method) tool ([11]) that incorporates the radial well geometry in detail, used in Chapter 5 for (steady state) radial well performance calculations, is extended to perform transient calculations. In Section 6.1 the well-known concept of *radius of influence* is explored which enables to incorporate ‘time’ into a steady state model with minor effort. This approach however is only approximate and has certain artefacts specially for the early part of the pressure transients. For that, a rigorous solution approach is investigated and implemented that solves accurately the transient pressure equation. This more involved approach is discussed in Section 6.2. Advantage of the followed approach is that it allows to include the effect of well bore storage (Section 6.2.1) and naturally extends to dual porosity reservoirs (not discussed here).

### 6.1 Radius of influence

Using the AEM, the Productivity Index  $PI$  for a radial well under steady state conditions is estimated, assuming a constant well pressure  $p_w$ , a constant reservoir pressure  $p_0$  at a reservoir radius  $r_e$ . The steady state well rate  $q$  is then found by

$$q = PI(r_e)(p_w - p_0) \quad (8)$$

Although  $PI$  is a function of many reservoir, well and fluid parameters, the dependency on reservoir radius is made explicit for the following discussion. In a simple but approximate way, time dependency can be incorporated in (8) using the well-known concept of *radius of influence* which we define here as the radial distance  $r_i$  for which  $p(r_i, t) = p_0$ ,  $p_0$  being the initial reservoir pressure and  $p(r_i, t)$  the pressure solution of a fully penetrated vertical well. This gives approximately  $r_i(t) = 1.5\sqrt{\eta t}$  with  $\eta = \frac{k}{\phi\mu c_t}$  the diffusivity coefficient<sup>1</sup> [14]. The radius of influence is the, in time increasing, radial distance of the affected region of the reservoir. To allow for pressure transient calculation we take  $r_e = r_e(t) = r_i(t)$  in (8).

<sup>1</sup>Several definitions exist of the radius of influence but they have in common the proportionality to  $\sqrt{\eta t}$ .

Version 6/8/2020	Upscaling of RJD for incorporation in reservoir simulators	page 16 / 41
------------------	--	--------------

For a drawdown (or injection) test,  $q$  is taken constant. The decline (buildup) of well pressure  $p_w = p_w(t)$  can then be calculated by

$$q = PI(r_e(t))(p_w(t) - p_0) \tag{9}$$

with

$$r_e(t) = 1.5\sqrt{\eta t} \tag{10}$$

Note that the calculation requires a sequence of steady state calculations for increasing reservoir radius  $r_e(t)$  values. This approach is expected only to be (approximately) correct if  $r_e(t)$  extends beyond the length of the radials, for early times therefore the solution will be inaccurate.

The approach using the radius of influence concept is tested on a radial well case with a configuration as shown in Figure A-1 and reservoir and fluid properties as given in Table A-1. In Figure 6-1 we compare AEM with the results of an Eclipse simulation of an *injection test*: after a shut-in period, the well pressure is build up due to a constant injection rate (3600 m<sup>3</sup>/d). The pressure buildup is well reproduced but the pressure derivative, see Figure 6-2, shows artefacts in early time such as the hump between 0.01 and 0.1 days. In this period the  $r_e$  grows to ~100 m (radial length) and beyond and radial flow has not yet been fully established.

Another immediate drawback of the approach is the inability to simulate a pressure falloff period when a well is shut-in after a buildup period.

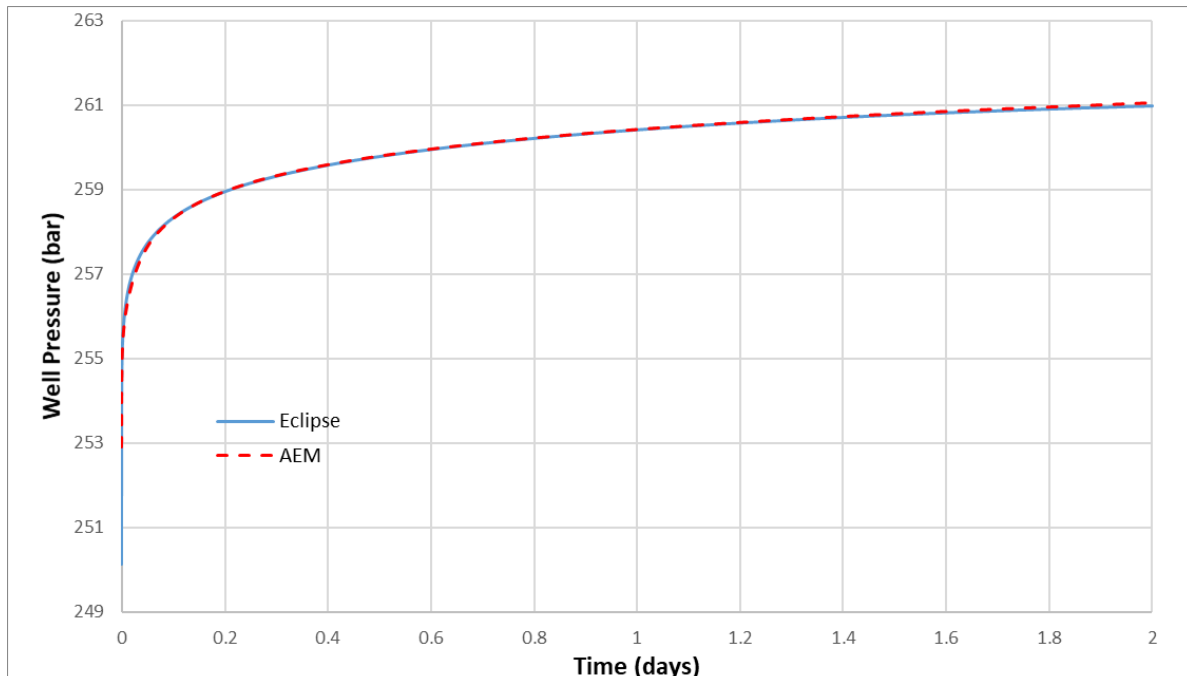


Figure 6-1. Comparison of pressure build up during injection test (constant rate of 3600 m<sup>3</sup>/day).

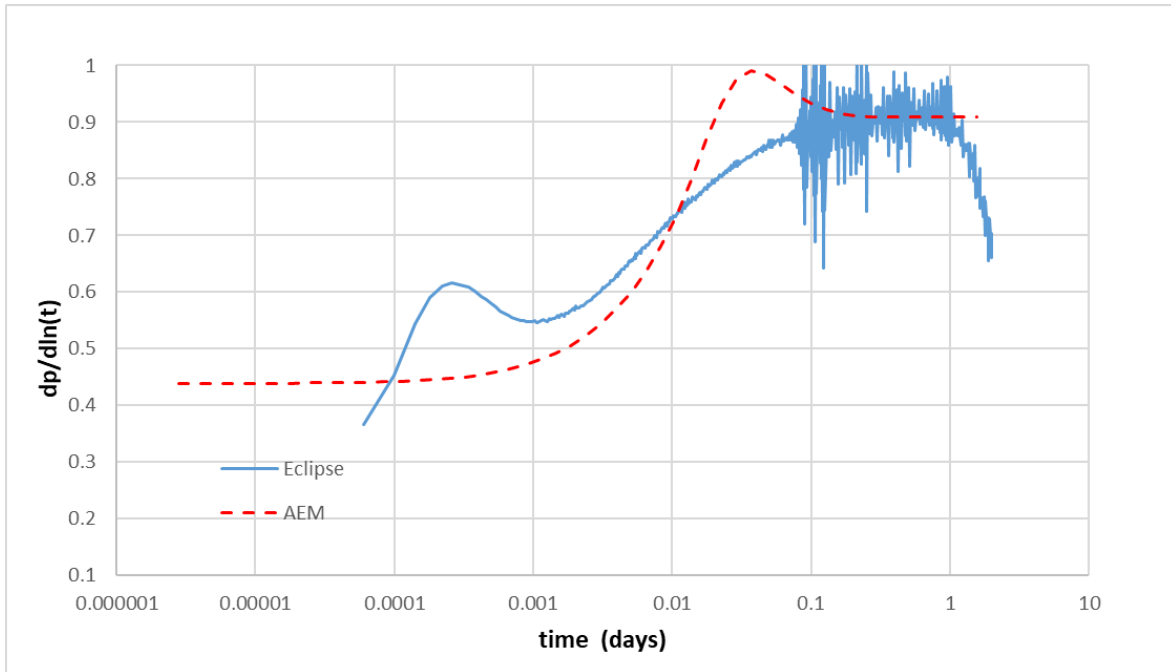


Figure 6-2. Comparison of the AEM with radius of influence approach and Eclipse of pressure build up during injection well test (constant rate of 3600 m<sup>3</sup>/day).

## 6.2 Transient solution

The drawbacks of the straightforward but approximate method using the radius of influence concept prompted the extension of the AEM tool to calculate the full pressure transient solution for a radial well. For that the diffusivity equation

$$\nabla^2 p = \frac{1}{\eta} \frac{\partial p}{\partial t} \quad (11)$$

needs to be solved with appropriate reservoir and well boundary conditions. Similarly, as we derived the steady state pressure solution for radial wells, a solution for the pressure field is constructed from 3D point source solutions exploiting the principle of superposition [16].

Although one may derive a transient point source solution by solving Eq. (11), we choose to solve the problem in the Laplace domain as the formulation and solution simplifies albeit at the cost of numerical Laplace inversion needed to arrive at a pressure solution in the time domain. Before applying the Laplace transform, Eq. (11) is rephrased using dimensionless time and space variables. Defining  $t_D = \frac{\eta}{r_w^2} t$  and  $r_D = \frac{r}{r_w}$ , with  $r_w$  the well radius and  $r$  the Euclidian distance, Eq. (11) becomes

$$\nabla_D^2 p = \frac{\partial p}{\partial t_D} \quad (12)$$

The Laplace transform  $\tilde{f}$  of a function  $f$  is defined by

$$\tilde{f}(s) = \int_0^{\infty} e^{-st} f(t) dt \quad (13)$$

with  $s$  a real or complex number.

Version 6/8/2020	Upscaling of RJD for incorporation in reservoir simulators	page 18 / 41
------------------	--	--------------

Applying the Laplace transform to (12) gives the simpler equation as the time derivative becomes a multiplication in the Laplace domain

$$\nabla_D^2 \tilde{p} = s\tilde{p} \quad (14)$$

of (14). A point source solution of (12) is given by

$$\tilde{p}(r_D, s) = q \frac{\mu}{4\pi k s r_w r_D} e^{-\sqrt{s} r_D} \quad (15)$$

Here  $q$ , in  $\text{m}^3/\text{sec}$ , is the continuous rate at a point source location  $x'$ ,  $\tilde{p}_D$  the solution at a point  $x$  and  $r_D = \frac{\|x-x'\|}{r_w}$ . In a similar fashion as the steady state solution is constructed for a radial well, the well is split up in a number of linear segments and for each segment a solution is derived through integration of point source solutions along the segment thereby allowing for a polynomially varying flux  $q$  along the segment ([9],[15], [16]). This integration is done numerically as no analytic solution was found. Using the principle of superposition, a pressure solution (in the Laplace domain) can be formed for the full radial well by summing up de solutions of the segments. As by construction, this solution will have multiple degrees of freedom, namely the coefficients of the polynomials describing the flux along the well, that can be exploited to satisfy a uniform pressure condition at distributed points along the well face. No-flow conditions at the top and bottom of the reservoir are obtained using the method of images.

Having constructed a pressure solution in the Laplace domain, to come back to the time domain, Laplace inversion is needed. A Laplace inversion method often used in well test literature is from Gaver-Stehfest [40]. This method expresses a function value at time  $t$  as a finite sum of weighted transformed function values, evaluated for only real values  $s$ . Typically, a function value can be calculated by 8-14 transformed function evaluations using double precision arithmetic.

### 6.2.1 Wellbore storage

For early times, wellbore storage effects should be accounted for to perform a proper well test interpretation [18]. A well test for which the rate at surface conditions is taken constant will not instantly result in a constant rate at reservoir conditions due to the presence of a compressible liquid inside the well bore. Effectively this means that the reservoir pressure equation for the reservoir needs to be solved with a time varying pressure boundary condition at the well-reservoir interface. This requires the coupling of the wellbore and reservoir pressure equations.

We will assume that the controllable *surface volume* well rate  $q_w^{surf}$  is taken constant and that the time dependent *reservoir volume* well rate  $q_w$  (at the reservoir depth) follows. The calculation of the reservoir volume well rate  $q_w$  needs to account for wellbore storage effects. Considering these effects, the well rate  $q_w = q_w(t)$  at reservoir depth is given by

$$q_w(t) = q_w^{surf} B_w - c_w V_w \frac{dp_w}{dt} \quad (16)$$

where  $B_w$  (res. Vol./surf. Vol.) is the formation volume factor,  $V_w$  the volume of the liquid in the well and  $c_w$  the compressibility of the liquid inside the well bore. In dimensionless time (16) converts to

$$q_w(t_D) = q_w^{surf} B_w - \frac{\eta}{r_w^2} c_w V_w \frac{dp_w}{dt_D}$$

Taking the Laplace transform (denoted by  $\sim$ ) gives

$$\tilde{q}_w(s) = \frac{q_w^{surf} B_w}{s} - \frac{\eta}{r_w^2} c_w V_w s \tilde{p}_w(s) \quad (17)$$

The constraint that the well operating at a reservoir volume rate is in AEM translated into a constraint through Eq. (17) for the unknowns describing the polynomial-shaped well influx along the well segments.

### 6.3 Results

#### 6.3.1 Radial well base case

The base case for the validation of the implementation of the transient AEM implementation is a radial well consisting of a fully penetrating vertical well with 4 orthogonal radials of length 100 m each with the same kickoff location at one-third of the well. The configuration is shown in Figure A-1. The radius  $r_w$  of the vertical well (backbone) is 0.1 m and the radii of the radial are 0.075 m. The well is producing during the test period at a constant surface volume rate of 3600 Sm<sup>3</sup>/day. It is further assumed that the pressure at the well face at reservoir depth is uniform. In case well bore storage (WBS) is included in the calculation a well volume  $V_w$  of 500 m<sup>3</sup> is taken and compressibility  $c_w$  of the water inside the well as given in Table 6-1.

At the lateral boundary of the reservoir a constant pressure is taken equal to the initial reservoir pressure. At the top and bottom of the reservoir a no-flow boundary condition is imposed. In Table 6-1 the reservoir and reservoir properties are listed.

Table 6-1. Reservoir and water properties.

Parameter	Description	Value
$p_i$	Initial reservoir pressure	25 MPa
$h$	Reservoir height	100 m
$r_e$	Reservoir radius	1134 m
$k_h$	Horizontal permeability	200 mD
$k_v$	Vertical permeability	20 mD
$\varphi$	Porosity	0.2
$\mu$	Water viscosity	0.54 cP
$c_w$	Water compressibility	3.28E-10 1/Pa
$c_t$	Total (water+rock) compressibility	8.2763E-10 1/Pa
$B_w$	Formation volume factor of water	1.0159 Rm <sup>3</sup> /Sm <sup>3</sup>
$q$	Surface volume well rate	3600 Sm <sup>3</sup> /day

The transient AEM is compared/validated with an Eclipse model with a fine scale grid permitting an explicit representation of the well. The Eclipse model is described in Appendix C.

### 6.3.2 Validation

The transient solution results of AEM are compared to an Eclipse simulation in Figure 6-3. In this figure the dimensionless pressure and its derivative are shown in a log-log plot. These are typical curves used for analyzing well tests, see e.g. [18]. The dimensionless variables used are

$$t_D = \frac{k_h / (\phi c_t \mu)}{r_w^2} t, \quad r_D = \frac{r}{r_w}$$

and

$$p_D(t_D, r_D) = \frac{2\pi k_h h}{q B_w \mu} (p(t, r) - p_0).$$

For the Laplace inversion of the pressure build up, the Gaver-Stehfest algorithm was used, using 8 transformed values to approximate a pressure value at a single time. It was found that taking 8 transformed values is computationally efficient and gives sufficiently accurate results.

We observe from Figure 6-3 that the validity of the transient solution extends to early times beyond the validity range of the Eclipse simulations. Also, the figure confirms that the observed hump in the radius of influence approach seen in Figure 6-2 is indeed an artefact.

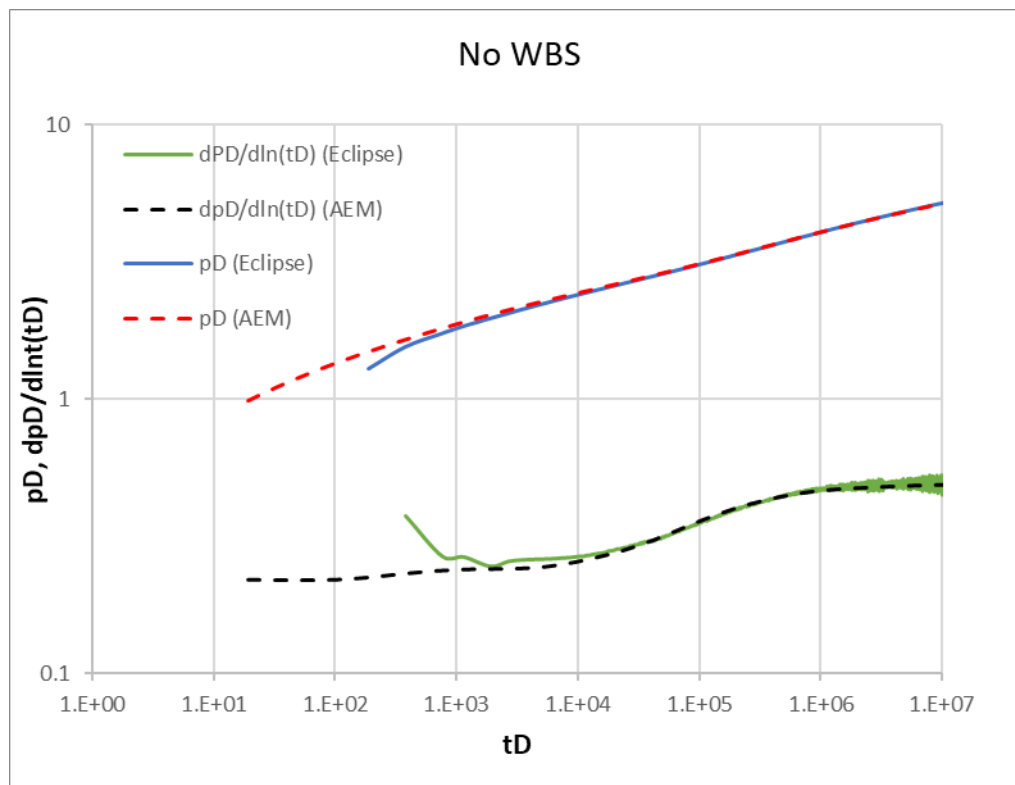


Figure 6-3. Comparison of AEM and Eclipse of the pressure buildup and its derivative during an injection test (constant rate). Wellbore storage (WBS) effects are not included.

In Figure 6-4 wellbore storage (WBS) is included in the simulations. For the pressure curve two linear slopes can be identified. The linear slope for early times is a manifestation of the domination of wellbore storage effect giving a linear relation between well pressure and time. Three time regions can be identified from the figure; initially a region where WBS dominates followed by a transition period between the WBS region and the region where radial flow has developed. The radial flow time region starts when the pressure derivative flattens.

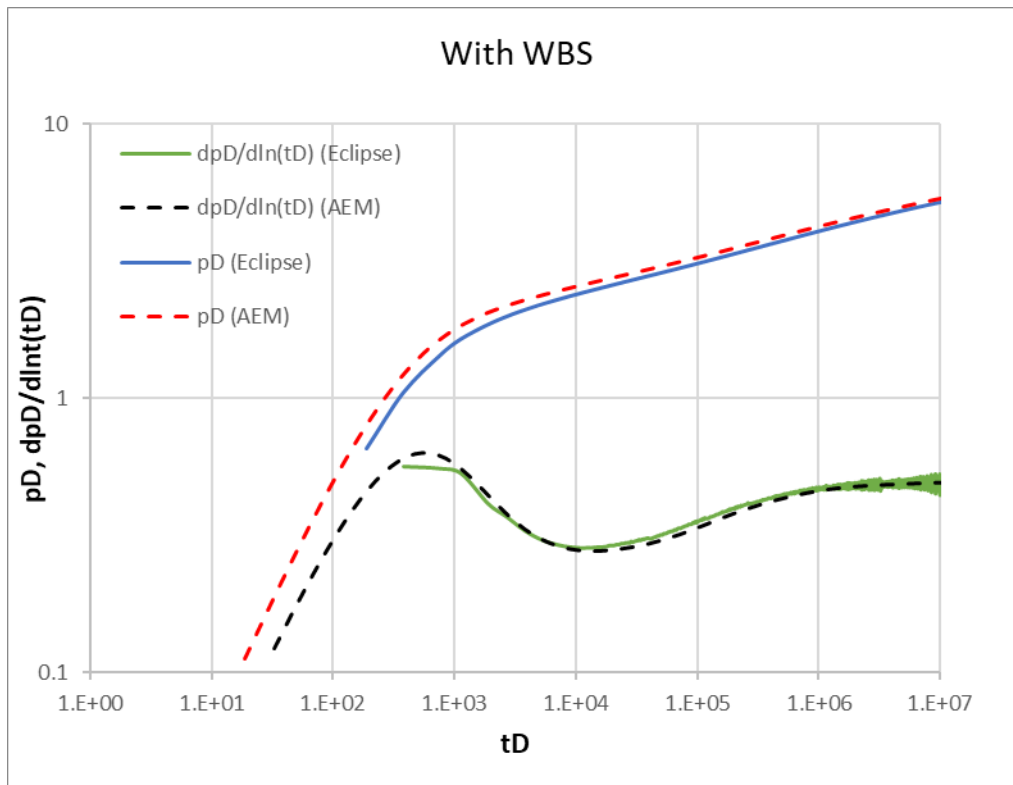


Figure 6-4. Comparison of AEM and Eclipse of the pressure buildup and its derivative during an injection test (constant rate). Wellbore storage (WBS) effects are included.

### 6.3.3 Well test type curves for radial wells

In this section we present some well test type curves obtained from the AEM simulations to illustrate the benefit of using this tool for interpretation of well tests results from radial wells. Because the jetting process is not steered, the position of the laterals in the reservoir is highly uncertain. By taking into account the laterals explicitly rather than as a skin, the well test response can be predicted much more accurately. For the simulations discussed below, we consider the base case radial well as described in Section 6.3.1.

In Figure 6-5 well test curves for increasing radial length are shown without well bore storage. In Figure 6-6 the same curves are shown with wellbore storage. Both figures clearly show that the development of radial flow, where the pressure derivative flattens, is later for longer radials as expected. These type curves can assist in analyzing well tests for radial wells and can give independent information about the actual length of the radials. Or more accurately, about how far the radials have been jetted away from the well. In particular, differences between a well test prior and after jetting can be interpreted to identify how far the radials reached away from the well. It should be noted that the observed dependency requires an explicit treatment of the geometry of the well in the simulations, as done by the AEM, and cannot be obtained by e.g. a transient model for a vertical well with a skin factor to represent the well's stimulation by jetted radials. The figures also illustrate the effect and relevance of including wellbore storage for early times.

In addition to the reach of the radials, also the number of radials strongly impacts the well test response. To illustrate this, type curves have been generated for an increasing number of radials. See Figure 6-7 for the used well configurations.

The type curves are shown in Figure 6-8. The development of radial flow occurs nearly at the same time for all well configurations except for the well without radials that shows a much earlier developed plateau of the pressure derivative. Obviously, the length of the radials determines the timing of radial flow development rather than the number of radials. Note also that the two well configurations with two radials cannot be distinguished from the figure as the curves are on top of each other.

Finally, in Figure 6-9 type curves are shown for varying inclination angle. The inclination angle is defined here as the angle between the radial and the horizontal plane taken positive clockwise; 0° gives horizontal radials, 40° gives downwardly pointing radials almost touching the bottom reservoir boundary. For the 40° case an earlier radial flow development can be observed. Otherwise, the results are similar to increasing numbers of radials, reflecting the increased inflow performance in the radials due to a higher exposure to the higher horizontal permeability.

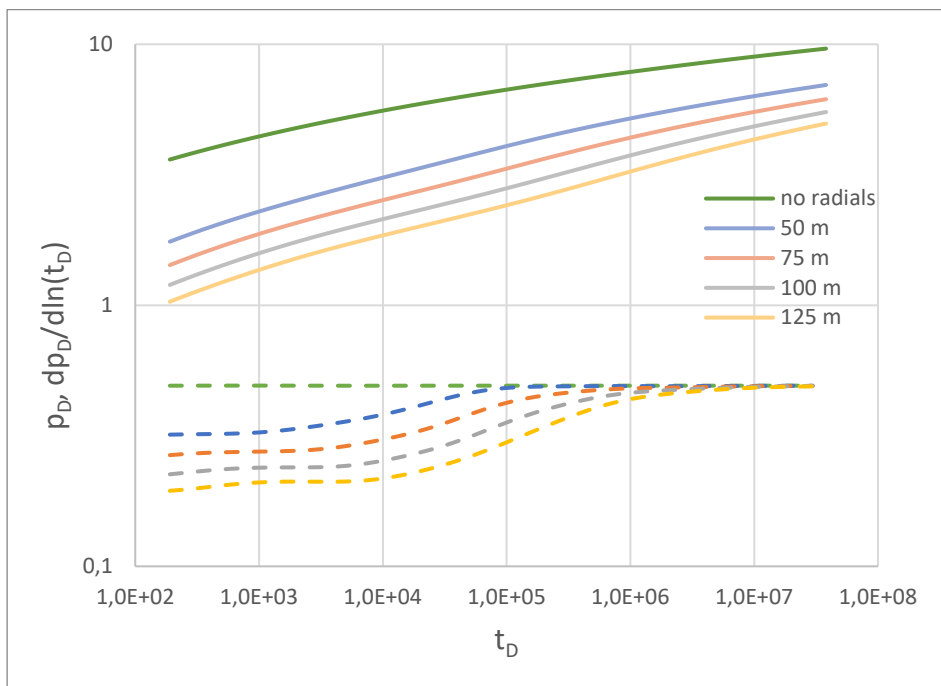


Figure 6-5. Pressure and pressure derivative (dashed lines) type curves for various lengths of the radials. No wellbore storage effects are included.

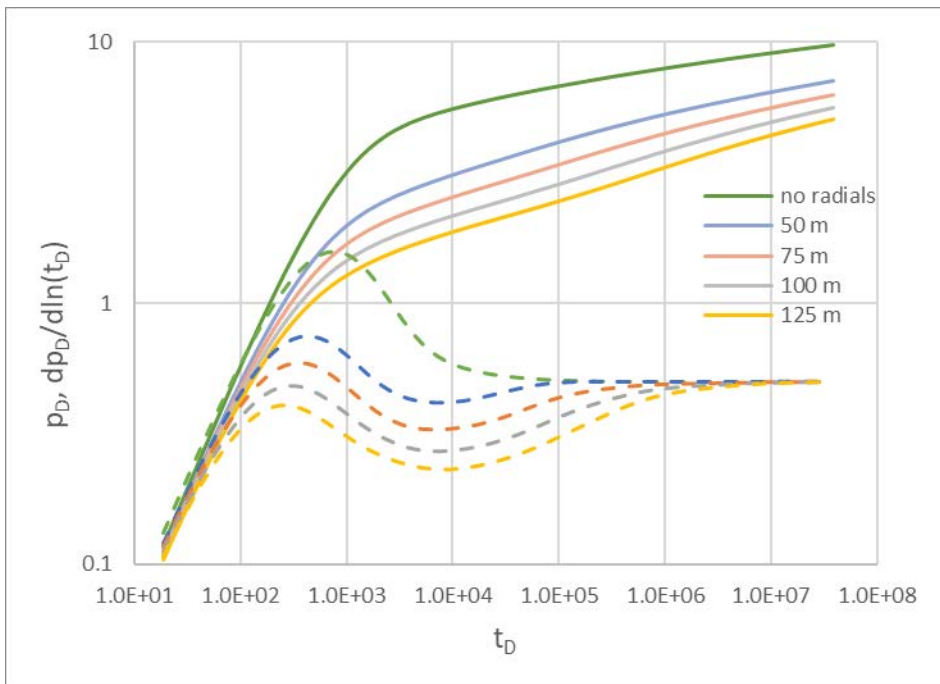


Figure 6-6. Pressure and pressure derivative (dashed lines) type curves for various lengths of the radials. Wellbore storage effects included.

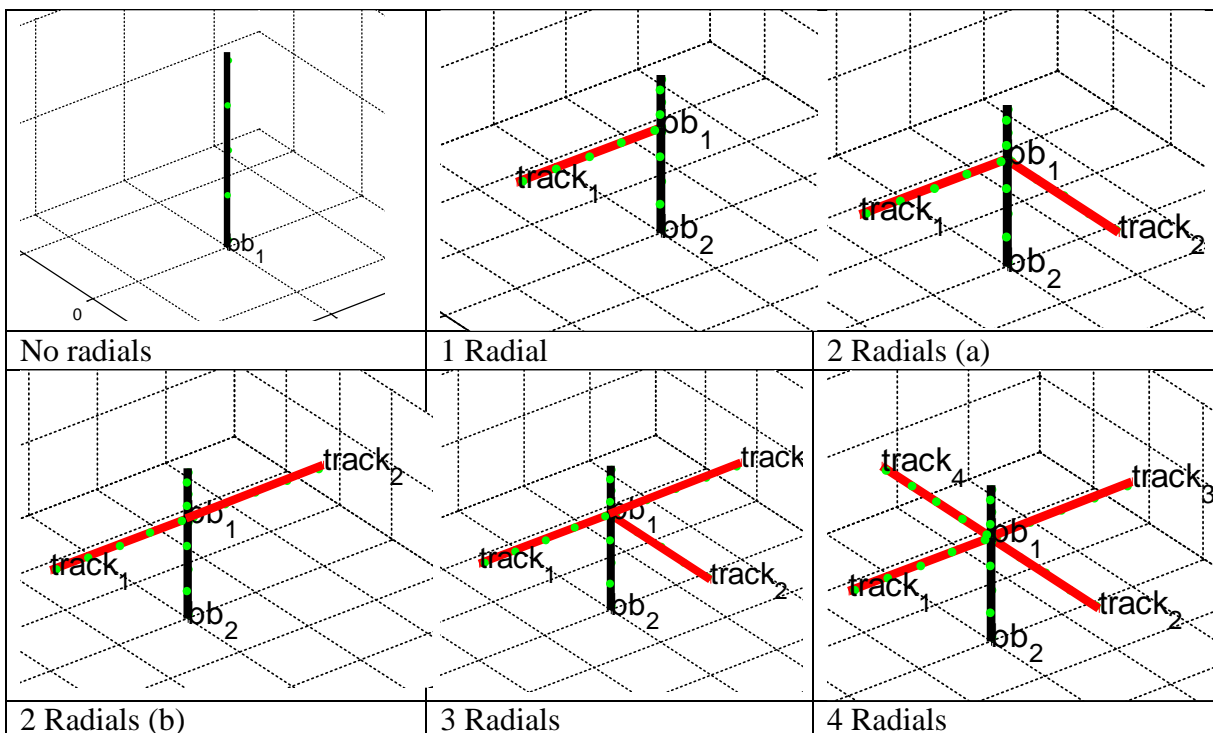


Figure 6-7. Radial well configurations used in Figure 6-8.

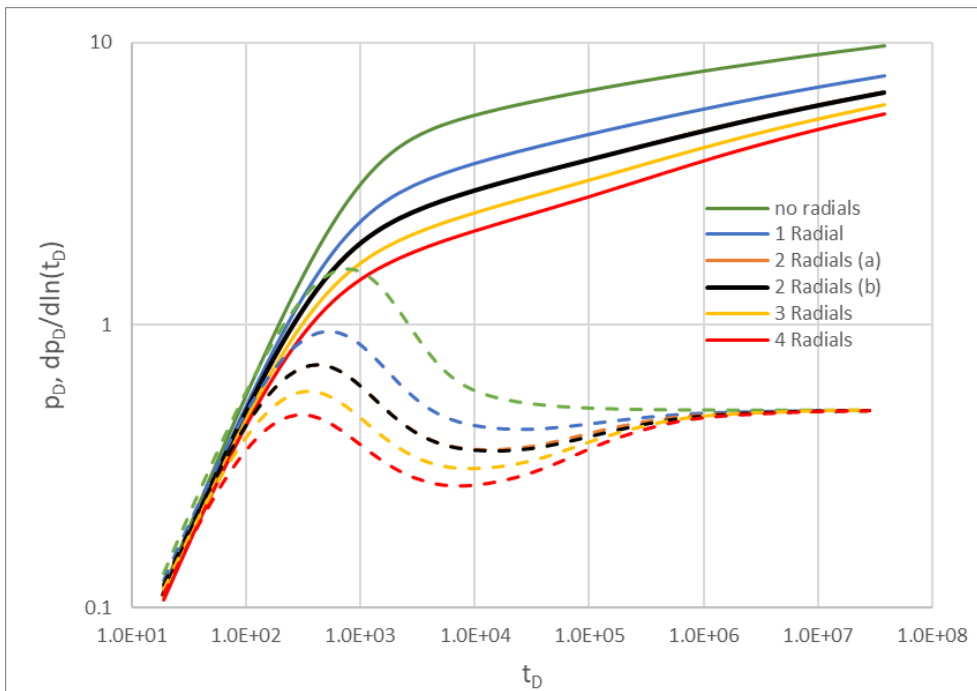


Figure 6-8. Pressure and pressure derivative (dashed lines) type curves for various number of radials, see Figure 6-7 for the well configurations.

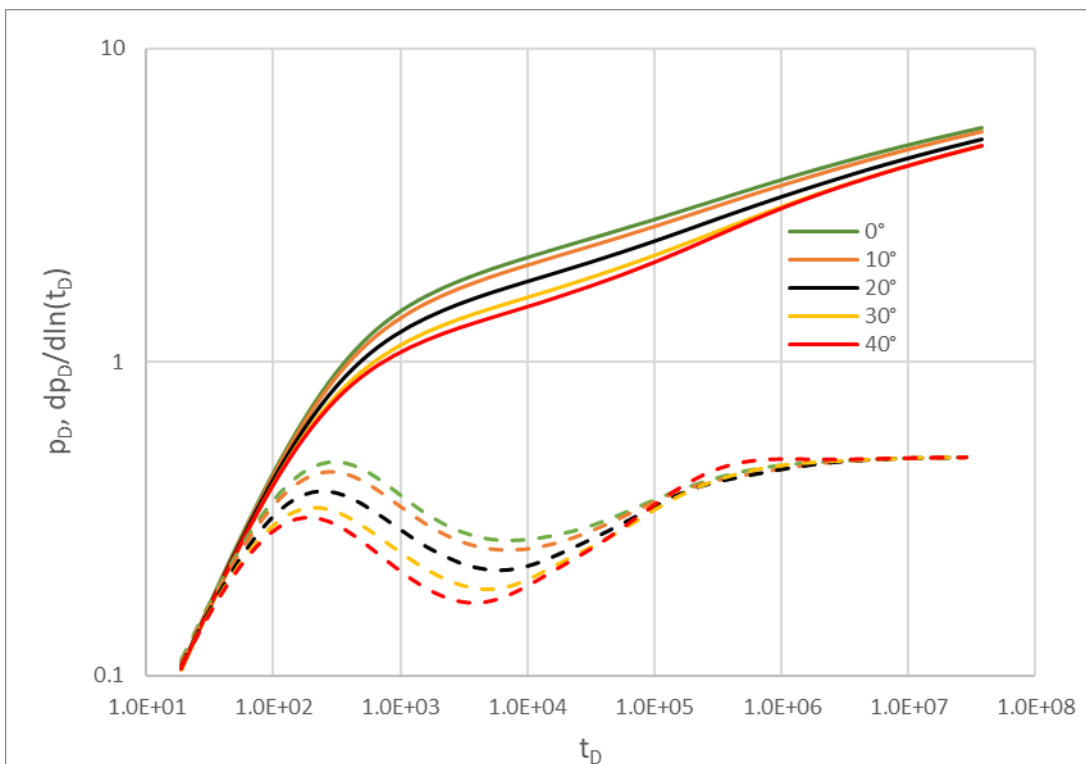


Figure 6-9. Pressure and pressure derivative (dashed lines) type curves for various inclinations.

## 7 Summary and conclusions

Prediction of the performance of well configurations obtained from Radial Jet Drilling (RJD) is imperative in the design phase of a radial well. Several, often numerical, methods exist that potentially can be used for such prediction. One of the goals of the presented work is to investigate what method(s) provide efficient and accurate simulations for radial wells on field scale. A complication of modeling well inflow (or outflow) using numerical methods is the large difference in dimensions of a well diameter and grid block sizes. For computational reasons an upscaling approach is often used that allows usage of relatively large grid blocks, compared to the well's diameter. An upscaling approach used in many numerical simulators is based on the well index concept. This widely used concept is further analyzed for the, complex radial well configurations.

A comparison was made between three numerical simulators and a semi-analytic approach. The underlying distinct approaches are the Finite Element Method with the well modeled explicitly by elements, the Finite Volume Method using the upscaling concept of well indices and the Analytic Element Method. It was found that simulators are mutually close with regard to the total flow rate but may differ considerably in how well inflow is distributed over the well segments (backbone and laterals).

For the purpose of the sensitivity analysis and optimization workflow developed and used in the connected tasks 7.5 and 7.6 of the project, the simulator based on the Finite Volume method was chosen because of the ability of upscaling, hence reducing CPU time. The accuracy of the FV approach was confirmed by the comparison study. The main purpose of these workflows is to support decisions concerning the design of the well in a robust way incorporating uncertainty in the reservoir description. As these workflows requires numerous simulations for many reservoir models and well configurations, automation is a necessity. To enable this, a tool was developed that calculates the well indices and grid block indices, needed by the simulator, from a geometrical description of the radial well, the grid definition and grid properties as permeabilities.

Besides using mathematical models for well performance prediction during the design phase, modelling may also assist in estimating well and reservoir characteristics after the implementation of the well in the field through interpretation of pressure transient data obtained from well tests. For that, the inhouse AEM tool was extended to derive the full pressure transient solution for a radial well including wellbore storage effects. A strength of the followed approach is that the geometry of the laterals is explicitly accounted for in contrast to standard approaches using a vertical or deviated well with a (negative) skin to incorporate well stimulation effects. Including the well geometry potentially allows to estimate the effectiveness of the jetting of the laterals, in particular the lateral reach may be highly uncertain. The semi-analytic approach was successfully validated with an Eclipse model with a very fine grid allowing to represent the well explicitly. As demonstration of the developed method several pressure and pressure derivative type curves for well test interpretation are shown.

## Acknowledgements

The research for this paper received funding from the European Union's Horizon 2020 research and innovation programme under grant agreement No. 654662 (SURE). The content of this poster reflects only the authors' view. The Innovation and Networks Executive Agency (INEA) is not responsible for any use that may be made of the information it contains. The

Version 6/8/2020	Upscaling of RJD for incorporation in reservoir simulators	page 26 / 41
------------------	--	--------------

help of the Norwegian University of Science and Technology (NTNU) with implementation of the WIC tool is gratefully acknowledged.

## Nomenclature

- $B_w$  = formation volume factor of water, [m<sup>3</sup>/m<sup>3</sup>]
- $c_t$  = total compressibility, [1/Pa]
- $c_w$  = compressibility of fluid in the well, [1/Pa]
- $h$  = reservoir height, [m]
- $k$  = permeability, [m<sup>2</sup>]
- $kh$  = permeability-thickness product, [m<sup>3</sup>]
- $l$  = well segment length, [m]
- $p$  = pressure, [Pa]
- $p_0$  = initial reservoir pressure, [Pa]
- $p_w$  = well pressure, [Pa]
- $PI$  = productivity index, [m<sup>3</sup>/s/Pa]
- $q$  = volumetric well rate, [m<sup>3</sup>/s]
- $q_w^{surf}$  = volumetric well rate at surface conditions [m<sup>3</sup>/s]
- $r$  = radial distance
- $r_{eq}$  = equivalent wellblock radius, [m]
- $r_i$  = radius of influence, [m]
- $r_w$  = well radius, [m]
- $r_e$  = external reservoir radius, [m]
- $s$  = Laplace variable
- $S$  = skin factor, [-]
- $t$  = time, [s]
- $V_w$  = the volume of the liquid in the well, [m<sup>3</sup>]
- $WI$  = well index, [m<sup>3</sup>] or [cP.rm<sup>3</sup>/day/bars] for Eclipse input
- $\gamma$  = Euler constant, [-]
- $\eta$  = diffusivity coefficient, [m<sup>2</sup>/s]
- $\mu$  = viscosity, [Pa s]
- $\phi$  = porosity, [-]
- $\psi$  = directional vector

## Subscripts

- $D$  = dimensionless parameter
- $i$  = gridblock index
- $x, y, z$  = the grid directions

## Table of Figures

Figure 2-1. Overview of well geometry created using radial jet drilling .....	4
Figure 3-1. WI calculated using the approach as described in TOUGH2 manual ([5], [29]) and following Peaceman. ....	8
Figure 3-2. Illustration of the projection approach. Red line is the well segment in the well block, the three blue lines are the projections on the permeability axis.....	9
Figure 4-1. From parametrization to reservoir simulation. ....	13
Figure 6-1. Comparison of pressure build up during injection test (constant rate of 3600 m <sup>3</sup> /day). ....	16
Figure 6-2. Comparison of the AEM with radius of influence approach and Eclipse of pressure build up during injection well test (constant rate of 3600 m <sup>3</sup> /day).....	17

Version 6/8/2020	Upscaling of RJD for incorporation in reservoir simulators	page 27 / 41
------------------	--	--------------

Figure 6-3. Comparison of AEM and Eclipse of the pressure buildup and its derivative during an injection test (constant rate). Wellbore storage (WBS) effects are not included..... 20

Figure 6-4. Comparison of AEM and Eclipse of the pressure buildup and its derivative during an injection test (constant rate). Wellbore storage (WBS) effects are included. .... 21

Figure 6-5. Pressure and pressure derivative (dashed lines) type curves for various lengths of the radials. No wellbore storage effects are included..... 22

Figure 6-6. Pressure and pressure derivative (dashed lines) type curves for various lengths of the radials. Wellbore storage effects included. .... 23

Figure 6-7. Radial well configurations used in Figure 6-8. .... 23

Figure 6-8. Pressure and pressure derivative (dashed lines) type curves for various number of radials, see Figure 6-7 for the well configurations..... 24

Figure 6-9. Pressure and pressure derivative (dashed lines) type curves for various inclinations. .... 24

Figure A-1. The radial well configuration..... 31

Figure C-1. Overview of the model setup with the radial well consisting of a vertical well with 4 perpendicular laterals. .... 39

**Table of Tables**

Table 6-1. Reservoir and water properties..... 19

Table A-1. Input settings of the calculation of options A, B and C for *WIt*. .... 30

Table A-2. Comparison of the results for *WIt* calculation methods A, B and C for a vertical well with 4 laterals of 50 m length. .... 31

Table A-3. Comparison of the results for *WIt* calculation methods A, B and C for a vertical well with 4 laterals of 20 m length (rate of semi-analytical tool is 2239.7 sm<sup>3</sup>/d). .... 32

Table A-4. Comparison of the results for *WIt* calculation methods A, B and C for the same setup but different numerical discretization (rate of semi-analytical tool is 2239.7 sm<sup>3</sup>/d).... 32

Table B-1. Comparison of well block indices and WI's calculated by the WIC tool and Petrel for Test 1..... 33

Table B-2. Comparison of well block indices and WI's calculated by the WIC tool and Petrel for Test 2..... 34

Table B-3. Comparison of well block indices and WI's calculated by the WIC tool and Petrel for Test 3..... 37

Table C-1. Grid size used in the model ..... 40

**References**

[1] Aavatsmark I., Klausen R.A.: Well Index in Reservoir Simulation for Slanted and Slightly Curved Wells in 3D Grids, SPE 75275, March 2003.

[2] Alvestad J, K. Holing, K. Christoffersen, O. Langeland and O. Stava: Interactive Modeling of Multiphase Inflow Performance of Horizontal and highly Deviated Wells, SPE 27577 presented at the 1994 SPE European Petroleum Computer Conference, Aberdeen, 15-17 March.

[3] Aziz K., Durlafsky L. and Tchelepi H. A.: Notes on Reservoir Simulation. Stanford University, Petroleum Engineering, July 2005.

- [4] Blodgett L. and Slack K. (ed.): 2009. Geothermal 101: Basics of Geothermal Energy Production and Use. GEOTHERMAL ENERGY ASSOCIATION, Washington D.C.
- [5] Coats, K.H.: Geothermal reservoir simulation. SPE-6892, presented at the 52<sup>nd</sup> Annual fall technical conference and exhibition of the SPE, Denver, Colorado, October 1977.
- [6] Cacace, M. and Jacquey, A.B.: Flexible parallel implicit modelling of coupled thermal-hydraulic-mechanical processes in fractured rocks, *Solid Earth*, 8, 921-941, <https://doi.org/10.5194/se-8-921-2017>, 2017.
- [7] Doe T., McLaren R., and Dershowitz W.: Discrete Fracture Network Simulations of Enhanced Geothermal Systems. PROCEEDINGS, Thirty-Ninth Workshop on Geothermal Reservoir Engineering. Stanford University, Stanford, California, February 24-26, 2014. SGP-TR-202.
- [8] Edwards, A.L.: TRUMP: A Computer Program for Transient and Steady State Temperature Distributions in Multidimensional Systems, National Technical Information Service, National Bureau of Standards, Springfield, VA. 1972
- [9] Egberts P.J.P. and Fokker P.A.: Analytic Modelling of Production into Complex Wells. Proceedings ECMOR VII, 2000
- [10] Egberts, P.J.P., Shatyrbaeva I., and Fokker P.A.: Well Inflow Modelling for Wells Not Aligned to a Numerical Grid. SPE 165986. Presented at SPE Reservoir Characterisation and Simulation Conference and Exhibition held in Abu Dhabi, UAE, 16–18 September 2013.
- [11] Egberts P.J.P. and Peters E.: A Fast Simulation Tool for Evaluation of Novel Well Stimulation techniques for Tight Gas Reservoirs. SPE 174289MS, presented at EAGE/Europec in Madrid in June 2015.
- [12] FEFLOW: <https://www.mikepoweredbydhi.com/products/feflow> FEFLOW-MIKE for deep geothermal (full commercial) (basis is a groundwater tool)
- [13] <https://github.com/PetroleumCyberneticsGroup/FieldOpt-WellIndexCalculator>. License: GNU Lesser Public License Version 3.
- [14] Fokker P.A., Brouwer G.K., and Verga F.: A Semi-Analytic Model for Productivity Testing of Multiple Wells. SPE 94153, presented at EAGE/Europec in Madrid in 2005.
- [15] Fokker P.A., Verga F., and Egberts P.J.P.: New Semi-analytic Technique to Determine Horizontal Well Productivity Index in Fractured Reservoirs, *SPE Reservoir Evaluation & Engineering* (April 2005), 123-131.
- [16] Fokker P.A., and Verga F.: A Semianalytic Model for the Productivity Testing of Multiple wells, *SPE Reservoir Evaluation & Engineering* (June2005), 466-477.
- [17] Gilman J.R.: Practical Aspects of Simulation of Fractured Reservoirs. International forum on reservoir simulation, 2003.
- [18] Gringarten A.C.: From Straight Lines to Deconvolution: The evolution of the State of the Art in Well Test Analysis, *SPE Reservoir Evaluation & Engineering* (February 2008) 53-62.
- [19] Guo B., Fu P., Hao Y., Peters C.A., and Carrigan C.R.: Thermal drawdown-induced flow channeling in a single fracture in EGS. *Geothermics* 61 (2016) 46–62. <http://dx.doi.org/10.1016/j.geothermics.2016.01.004>.
- [20] <https://www.pipeflowcalculations.net/pressuredrop.xhtml>, access date 6-11-2018.
- [21] Matthäi S.K., Geiger, S., Roberts, S.G. 2001. The complex systems platform csp3.0: Users guide. Technical report, ETH Zürich Research Reports.
- [22] Narasimhan T.N. and Witherspoon P.A.: An Integrated Finite Difference Method for Analyzing Fluid Flow in Porous Media, *Water Resour. Res.*, Vol. 12, No. 1, pp. 57 – 64, 1976.

- [23] O’Sullivan M.J.: Geothermal Fluid Dynamics, 17<sup>th</sup> Australasian Fluid Mechanics Conference, Auckland, New Zealand, 5-9 December 2010
- [24] PANDAS - Parallel Adaptive static/dynamic Nonlinear Deformation Analysis System (fractured media, FEM), Enhanced Geothermal Reservoir Simulation. Huilin Xing, Ji Zhang, Yan Liu, Hans Mulhaus. The University of Queensland, Earth System Science Computational Centre, St Lucia, QLD 4072.
- [25] Peaceman D.W.: Interpretation of Well-Block Pressures in Numerical Reservoir Simulation, SPE 6893, June 1978.
- [26] Peaceman D.W.: Interpretation of Well-Block Pressures in Numerical Reservoir Simulation with Nonsquare Gridblocks and Anisotropic Permeability, SPE 10528, December 1983.
- [27] Peaceman D.W.: A new method for representing multiple wells with arbitrary rates in numerical reservoir simulation. SPE 29120-PA. SPE- 29120-PA. <https://doi.org/10.2118/29120-PA>, 1995.
- [28] Peters, E., Blöcher, G., Salimzadeh, S., Egberts, P. J. P., and Cacace, M.: Modelling of multi-lateral well geometries for geothermal applications, Adv. Geosci., 45, 209-215, <https://doi.org/10.5194/adgeo-45-209-2018>, 2018.
- [29] Pruess, K., C. Oldenburg and G. Moridis: TOUGH2 User’s guide, Version 2. LBNL-43134. Lawrence Berkeley National Laboratory. 2012
- [30] Reinsch, T., Paap, B., Hahn, S., Wittig, V. and van den Berg, S: Insights Into the Radial Water Jet Drilling Technology - Application in a Quarry. Doi: 10.1016/j.jrmge.2018.02.001. 2018.
- [31] Rozon, B.J.: A Generalized Finite Volume Discretization Method for Reservoir Simulation. Presented at the SPE Symposium on Reservoir Simulation, Houston, Texas, 6-8 February 1989. SPE-18414-MS. <http://dx.doi.org/10.2118/18414-MS>
- [32] Salimzadeh et al.: Tested and validated models for RJD well flow improvement. SURE deliverable D7.3. in preparation.
- [33] Schlumberger, 2017. Petrel User Assistance, October 2017.
- [34] Schlumberger, 2018. ECLIPSE: “Schedule User Guide 2018.1”, Chapter 6 “Technical Description 2018.1
- [35] SHEMAT (Aachen: Proceedings European Geothermal Congress 2007) finite difference solution
- [36] Shu J.: Comparison of various techniques for computing Well Index, Report Stanford University, August 2005.
- [37] STARS (CMG, <https://www.cmgl.ca/stars>)
- [38] TETRAD (ThinkGeoEnergy, <http://www.thinkgeoenergy.com/tag/tetrad/>)
- [39] Vaccaro M., and Conti P.: Numerical simulation of geothermal resources: a critical overlook, European Geothermal Congress 2013, Pisa, Italy 3-7 June 2013.
- [40] Valko P.P., and Abate J.: Numerical Laplace inversion in rheological characterization, J. Non-Newtonian Fluid Mech. 116 (2004) 395-406.
- [41] Wolfsteiner C., Durlofsky L.J. and Aziz K.: Calculation of well index for nonconventional wells on arbitrary grids. Computational Geosciences 7: 61–82, 2003.
- [42] Yeh A., Boyce-Bacon J., and O’Sullivan M.: Review of Deliverability Models Used in Geothermal Reservoir Simulations. Proceedings World Geothermal Congress 2015, Melbourne, Australia, 19-25 April 2015.

**Appendix A. Evaluation of WI amalgamation options.**

The three formulations for WI (Chapter 4) result in different values for  $WI$ . Consider for example the typical configuration shown in Figure A-1, of a vertical backbone with 4 horizontal laterals. As an example, we will calculate  $WI_t$  for a grid of 20 x 20 x 5 m with horizontal permeability of 200 mD. Further input can be found in Table A-1. The laterals are 50 m long. In Table A-2,  $WI_t$  for options A, B and C is presented for this configuration. The relative difference between the smallest and largest  $WI_t$  for the well block that contains the kickoff point, is 111%. For the WIs summed of the entire well ( $\sum_{j=1}^n WI_j$ , where  $n$  is the number of connection for a well) the difference is 8.7%. For the total flow from the well, the difference between options A and C is only 0.7 % (Table A-2). The reason for the small difference in total flow is that inflow into the well block in which the connection between the laterals and backbone occurs, receives very little flow because it is at the center of the well. The difference between the three options A, B and C for the calculation of WI is in fact smaller than the numerical accuracy of the simulator: the same configuration simulated with a semi-analytical solution gives a rate of 2615 sm<sup>3</sup>/d, which is 1.9 % different from the average rate of options A, B and C. This numerical inaccuracy is also clear from the increase in rate due to the laterals: 28.3 % for the semi-analytical solution and 31.2 to 30.2 % for options A and C respectively. See Chapter 5 for an explanation of the semi-analytical method and an analysis of the accuracy of different simulators.

*Table A-1. Input settings of the calculation of options A, B and C for  $WI_t$ .*

Grid size	20 x 20 x 5 m
Reservoir dimensions	2020 x 2020 x 100 m
Lateral boundary conditions	Constant pressure
Position of the vertical well	1005 x 1005 m
Horizontal permeability	200 mD
Vertical permeability	20 mD
Porosity	0.2
Diameter backbone and laterals	0.1524 m
Water viscosity	0.54 cP
Formation volume factor of water	1.0159 Rm <sup>3</sup> /Sm <sup>3</sup>

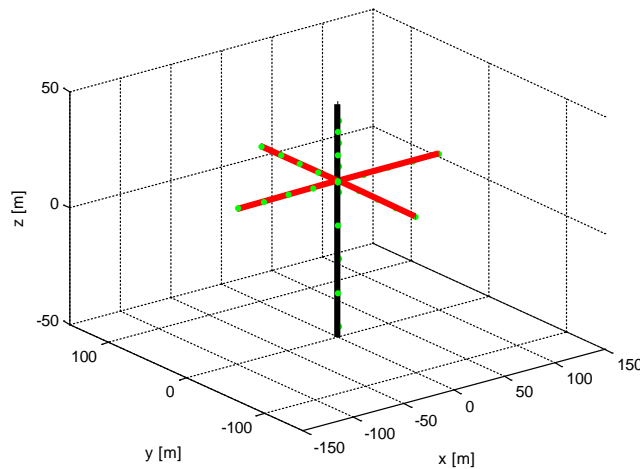


Figure A-1. The radial well configuration.

Table A-2. Comparison of the results for  $WI_t$  calculation methods A, B and C for a vertical well with 4 laterals of 50 m length.

	Option A	Option B	Option C
$WI_t$ well block [cP.rm <sup>3</sup> /day/bars]	57.1	33.6	16.3
$WI$ of the well [cP.rm <sup>3</sup> /day/bars]	488.9	465.4	448.1
Steady state rate @ 10 bar pressure difference (sm <sup>3</sup> )	2674.8	2665.8	2654.9
Increase in rate due the laterals (sm <sup>3</sup> /d)	635.9	626.9	616.1

For the typical example discussed above, the impact of the WI calculation method is negligible compared to the numerical accuracy. However, this might not be the case for other examples. Examples where the WI calculation method could have a larger impact, is when the well block in which the connections are located, is more important for the total WI. Therefore we analyse the same case, but with 20 m long laterals instead of 50 m long (Table A-3). The grid resolution of 20 m is very coarse for such a well, because it is in the same order as the length of the laterals. The difference in the flow rate of the well between options A, B and C is now 1.8% and for the increase in rate even 19%. The rate calculated with the semi-analytical tool is 2239.7 sm<sup>3</sup>/d, which is about mid-way between options B and C. However, changing the numerical definition of the problem a bit, by for example putting the well exactly in the centre of the grid block or by decreasing the grid size to 10 m instead of 20 m, changes the results considerably (Table A-4). For example, for the results of the finer grid, the three options come closer together, but differ slightly more from the semi-analytical solution.

Version 6/8/2020	Upscaling of RJD for incorporation in reservoir simulators	page 32 / 41
------------------	--	--------------

Table A-3. Comparison of the results for  $WI_t$  calculation methods A, B and C for a vertical well with 4 laterals of 20 m length (rate of semi-analytical tool is 2239.7  $sm^3/d$ ).

	Option A	Option B	Option C
$WI_t$ well block [cP.rm <sup>3</sup> /day/bars]	57.1	33.6	16.3
$WI$ of the well [cP.rm <sup>3</sup> /day/bars]	358.3	334.8	317.5
Steady state rate @ 10 bar pressure difference (sm <sup>3</sup> )	2271.1	2252.0	2228.8
Increase in rate due the laterals (sm <sup>3</sup> /d)	232.2	213.1	189.9

Table A-4. Comparison of the results for  $WI_t$  calculation methods A, B and C for the same setup but different numerical discretization (rate of semi-analytical tool is 2239.7  $sm^3/d$ ).

	Option A	Option B	Option C
Steady state rate @ 10 bar pressure difference (sm <sup>3</sup> ) for centred well	2276.7	2258.1	2235.3
Steady state rate @ 10 bar pressure difference (sm <sup>3</sup> ) for 10 m grid size	2267.6	2264.2	2258.5

**Appendix B. Running and testing of the WIC tool**

A range of cases was used to test whether the WIC tool gives accurate results. For simple cases the results can be checked manually. For more complicated cases, the results are compared to the WI calculations of Petrel<sup>2</sup>, which are assumed to be accurate.

Three tests are defined:

- Test 1: vertical well with horizontal laterals in rectangular grid
- Test 2: deviated well with laterals in rectangular grid
- Test 3: deviated well in non-rectangular dual-porosity grid.

As the tool is still under development, not all options are supported. Currently dual porosity, inactive grid blocks and skin on the well are supported. The use of NTG for the WI calculation is not supported (neither for  $kh$  nor  $r_{eq}$ ). Pinch-outs and crossing of faults has not been tested. Wells with strong curvature may result in deviations from the correct result, because the well needs to be approximated by linear segments. Also all well segments need to be defined with increasing coordinates in the current version of the tool: for example defining a segment pointing upwards may result in calculation of wrong WI at the tip. Preferably all well parts should be inside the grid.

Version tested 26-1-2018.

The input required to run the WIC tool is:

- Consistent EGRID and INIT file (both from Eclipse to ensure identical inactive blocks and the same number of active grid blocks)
- File with linear well segments (defined with increasing coordinates)

Test 1.

Grid size: 201 x 201 x 40 rectangular grid. The vertical well or backbone (bb) is located in block 101, 101 and has 40 connections. Each lateral has 11 connections: 5 m connection where it connects to the backbone, 9 times 10 m and 1 final connection of 5 m. In the table below only a single lateral is presented. The WI in the well block in which the laterals are connected to the backbone is smaller in the WIC tool because of a difference in calculation method. For explanations see Chapter 4.

*Table B-1. Comparison of well block indices and WI's calculated by the WIC tool and Petrel for Test 1.*

Well part	Petrel				WIC tool			
	x	y	z	WI (cP.rm <sup>3</sup> /day/bar)	x	y	z	WI (cP.rm <sup>3</sup> /day/bar)
bb	101	101	1	8.2238	101	101	1	8.22375
bb			:				:	
bb	101	101	13	8.2338	101	101	13	8.22375
bb	101	101	14	27.48*	101	101	14	15.9071*
bb	101	101	15	8.2338	101	101	15	8.22375
bb			:				:	
bb	101	101	40	8.2338	101	101	40	8.22375
l1	101	100	14	9.6283	101	100	14	9.62826
		:				:		
l1	101	92	14	9.6283	101	92	14	9.62826

<sup>2</sup> In Petrel a well index is called 'connection transmissibility factor'

Version 6/8/2020	Upscaling of RJD for incorporation in reservoir simulators	page 34 / 41
------------------	--	--------------

11	101	91	14	4.8141	101	91	14	4.81413
----	-----	----	----	--------	-----	----	----	---------

\* well block in which the laterals are connected to the backbone.

Test 2

For Test 2 the complete COMPDAT section for Eclipse is reproduced. The well block indices and WI's of the purely horizontal and vertical parts of the well (L2 and L4) calculated by the WIC tool are exactly the same as in Petrel, the deviated parts of the well shows small differences.

Table B-2. Comparison of well block indices and WI's calculated by the WIC tool and Petrel for Test 2.

Well part	Petrel				WIC tool			
	x	y	z	WI (cP.rm <sup>3</sup> /day/bar)	x	y	z	WI (cP.rm <sup>3</sup> /day/bar)
bb	98	101	1	8.5817	98	101	1	8.58104
bb	98	101	2	8.5817	98	101	2	8.58104
bb	98	101	3	8.5817	98	101	3	8.58104
bb	98	101	4	8.5811	98	101	4	8.58104
bb	98	101	5	8.5808	98	101	5	8.58104
bb	98	101	6	6.0953	98	101	6	6.11478
bb	99	101	6	2.4856	99	101	6	2.46626
bb	99	101	7	8.5808	99	101	7	8.58104
bb	99	101	8	8.5808	99	101	8	8.58104
bb	99	101	9	8.5808	99	101	9	8.58104
bb	99	101	10	8.5808	99	101	10	8.58104
bb	99	101	11	8.5808	99	101	11	8.58104
bb	99	101	12	3.6445	99	101	12	3.64852
bb	100	101	12	11.07	100	101	12	10.9964
bb	100	101	13	15.626	100	101	13	15.5327
bb	100	101	14	24.765	100	101	14	17.865
bb	100	101	15	8.5808	100	101	15	8.58104
bb	100	101	16	8.5808	100	101	16	8.58104
bb	100	101	17	8.5808	100	101	17	8.58104
bb	100	101	18	1.1938	100	101	18	1.18226
bb	101	101	18	7.387	101	101	18	7.39878
bb	101	101	19	8.5808	101	101	19	8.58104
bb	101	101	20	8.5808	101	101	20	8.58104
bb	101	101	21	8.5808	101	101	21	8.58104
bb	101	101	22	8.5808	101	101	22	8.58104
bb	101	101	23	7.3239	101	101	23	7.29705
bb	102	101	23	1.2569	102	101	23	1.284
bb	102	101	24	8.5808	102	101	24	8.58104
bb	102	101	25	8.5808	102	101	25	8.58104
bb	102	101	26	8.5808	102	101	26	8.58104
bb	102	101	27	8.5808	102	101	27	8.58104

bb	102	101	28	8.5808	102	101	28	8.58104
bb	102	101	29	4.8732	102	101	29	4.83079
bb	103	101	29	3.7076	103	101	29	3.75026
bb	103	101	30	8.5808	103	101	30	8.58104
bb	103	101	31	8.5808	103	101	31	8.58104
bb	103	101	32	8.5808	103	101	32	8.58104
bb	103	101	33	8.5808	103	101	33	8.58104
bb	103	101	34	8.5805	103	101	34	8.58104
bb	103	101	35	2.4283	103	101	35	2.36453
bb	104	101	35	6.1522	104	101	35	6.21652
bb	104	101	36	8.5805	104	101	36	8.58104
bb	104	101	37	8.5805	104	101	37	8.58104
bb	104	101	38	8.5805	104	101	38	8.58104
bb	104	101	39	8.5805	104	101	39	8.58104
bb	104	101	40	8.5805	104	101	40	8.36325
L1*	101	101	12	0.91087	104	101	1	7.0438
L1	101	101	11	7.0448	104	101	2	7.04529
L1	101	101	10	7.0448	104	101	3	5.12483
L1	101	101	9	4.7369	103	101	3	1.92046
L1	102	101	9	2.3079	103	101	4	7.04529
L1	102	101	8	7.0448	103	101	5	7.04529
L1	102	101	7	7.0448	103	101	6	3.72162
L1	102	101	6	3.3398	102	101	6	3.32367
L1	103	101	6	3.705	102	101	7	7.04529
L1	103	101	5	7.0448	102	101	8	7.04529
L1	103	101	4	7.0448	102	101	9	2.31841
L1	103	101	3	1.9427	101	101	9	4.72687
L1	104	101	3	5.1021	101	101	10	7.04529
L1	104	101	2	7.0448	101	101	11	7.04529
L1	104	101	1	7.0448	101	101	12	0.915203
L2	100	102	14	9.6283	100	102	14	9.62826
L2	100	103	14	9.6283	100	103	14	9.62826
L2	100	104	14	9.6283	100	104	14	9.62826
L2	100	105	14	9.6283	100	105	14	9.62826
L2	100	106	14	9.6283	100	106	14	9.62826
L2	100	107	14	9.6283	100	107	14	9.62826
L2	100	108	14	9.6283	100	108	14	9.62826
L2	100	109	14	9.6283	100	109	14	9.62826
L2	100	110	14	9.6283	100	110	14	9.62826
L2	100	111	14	4.8141	100	111	14	4.81413
L3	99	101	14	0.48983	99	101	14	0.488005
L3	99	101	15	7.0458	99	101	15	7.04529
L3	99	101	16	7.0458	99	101	16	7.04529
L3	99	101	17	5.1466	99	101	17	5.15407

L3	98	101	17	1.8992	98	101	17	1.89121
L3	98	101	18	7.0458	98	101	18	7.04529
L3	98	101	19	7.0458	98	101	19	7.04529
L3	98	101	20	3.7373	98	101	20	3.75086
L3	97	101	20	3.3085	97	101	20	3.29442
L3	97	101	21	7.0458	97	101	21	7.04529
L3	97	101	22	7.0458	97	101	22	7.04529
L3	97	101	23	2.3279	97	101	23	2.34765
L3	96	101	23	4.7179	96	101	23	4.69763
L3	96	101	24	7.0458	96	101	24	7.04529
L3	96	101	25	7.0458	96	101	25	7.04529
L3	96	101	26	0.91856	96	101	26	0.944446
L3	95	101	26	6.1273	95	101	26	6.10084
L3	95	101	27	7.0458	95	101	27	7.04529
L3	95	101	28	6.555	95	101	28	6.58652
L3	94	101	28	0.4908	94	101	28	0.458763
L3	94	101	29	7.0458	94	101	29	7.04529
L3	94	101	30	7.0458	94	101	30	7.04529
L3	94	101	31	5.1457	94	101	31	5.18332
L3	93	101	31	1.9002	93	101	31	1.86197
L3	93	101	32	7.0458	93	101	32	7.04529
L3	93	101	33	7.0458	93	101	33	7.04529
L3	93	101	34	3.7363	93	101	34	3.78011
L3	92	101	34	3.3095	92	101	34	3.26518
L3	92	101	35	7.0458	92	101	35	7.04529
L3	92	101	36	7.0458	92	101	36	7.04529
L3	92	101	37	0.31564	92	101	37	0.348671
L4	100	100	14	9.6283	100	100	14	9.62826
L4	100	99	14	9.6283	100	99	14	9.62826
L4	100	98	14	9.6283	100	98	14	9.62826
L4	100	97	14	9.6283	100	97	14	9.62826
L4	100	96	14	9.6283	100	96	14	9.62826
L4	100	95	14	9.6283	100	95	14	9.62826
L4	100	94	14	9.6283	100	94	14	9.62826
L4	100	93	14	9.6283	100	93	14	9.62826
L4	100	92	14	9.6283	100	92	14	9.62826
L4	100	91	14	4.8141	100	91	14	4.81413

\* The ordering for L1 is reverse in the WIC tool because segments need to be defined with increasing values.

### Test 3

Dual porosity case with deviated well: for most WI values, the difference between the WI from Petrel and the WIC tool is less than 10%. For the first and last block of the well, larger differences occur. This is due to a bug in the calculation of the intersections of the grid block

faces that has not been fixed at the moment of writing this report. For a sufficiently fine grid, the impact of this bug is small, because it affects only a single well block.

Table B-3. Comparison of well block indices and WI's calculated by the WIC tool and Petrel for Test 3.

Petrel				WIC tool			
x	y	z	WI (cP.rm <sup>3</sup> /day/bar)	x	y	z	WI (cP.rm <sup>3</sup> /day/bar)
117	101	13	0.584981	117	101	13	0.469486
117	101	54	0.050108	117	101	54	0.036627
117	101	14	0.604327	117	101	14	0.613132
117	101	55	0.051018	117	101	55	0.048021
117	101	15	0.603307	117	101	15	0.611609
117	101	56	0.051347	117	101	56	0.048379
117	101	16	0.602266	117	101	16	0.610102
117	101	57	0.051726	117	101	57	0.048772
117	101	17	0.601236	117	101	17	0.608594
117	101	58	0.0521	117	101	58	0.048896
117	101	18	0.600187	117	101	18	0.607112
117	101	59	0.052464	117	101	59	0.049308
117	101	19	0.599169	117	101	19	0.605631
117	101	60	0.052822	117	101	60	0.049731
117	101	20	0.598111	117	101	20	0.604139
117	101	61	0.053167	117	101	61	0.050158
117	101	21	0.001816	117	101	21	0.005183
117	101	62	0.001816	117	101	62	0.005183
117	101	22	0.015709	117	101	22	0.015864
117	101	63	0.151706	117	101	63	0.145864
116	101	22	0.007322	116	101	22	0.006361
116	101	63	0.092708	116	101	63	0.081931
116	101	23	0.024108	116	101	23	0.024203
116	101	64	0.318154	116	101	64	0.325055
116	101	24	0.024235	116	101	24	0.024318
116	101	65	0.33271	116	101	65	0.339989
116	101	25	0.024783	116	101	25	0.024437
116	101	66	0.355971	116	101	66	0.357705
116	101	26	0.024915	116	101	26	0.02456
116	101	67	0.373625	116	101	67	0.375711
116	101	27	0.025051	116	101	27	0.024687
116	101	68	0.391507	116	101	68	0.392981
116	101	28	0.018311	116	101	28	0.018053
116	101	69	0.299702	116	101	69	0.301341
115	101	28	0.00686	115	101	28	0.006843
115	101	69	0.162315	115	101	69	0.174399

Version 6/8/2020	Upscaling of RJD for incorporation in reservoir simulators	page 38 / 41
------------------	--	-----------------

115	101	29	0.025262	115	101	29	0.02517
115	101	70	0.628256	115	101	70	0.675033
115	101	30	0.025411	115	101	30	0.025324
115	101	71	0.662347	115	101	71	0.712116
115	101	31	0.025565	115	101	31	0.025483
115	101	72	0.696375	115	101	72	0.749586
115	101	32	0.049499	115	101	32	0.049259
115	101	73	1.42822	115	101	73	1.51896
114	101	32	0.013687	114	101	32	0.013988
114	101	73	0.580212	114	101	73	0.637934
114	101	33	0.065218	114	101	33	0.065675
114	101	74	3.08951	114	101	74	3.34982
114	101	34	0.040362	114	101	34	0.040701
114	101	75	2.14143	114	101	75	2.32587
113	101	34	9.86E-05	113	101	34	0.026817
113	101	75	0.007482	113	101	75	2.18433

**Appendix C. Eclipse model used for simulating well testing**

The properties and setup of the well are the same as those used in Chapter 5 and Appendix B: a fully penetrating vertical well (backbone) with 4 horizontal laterals at 33 m from the top. In this case however, the well and laterals are modelled explicitly using fine grid blocks with high permeability. The size of the grid blocks representing the well determines the well diameter and thus has to be taken small. This results in a large number of grid blocks for the entire model. To reduce CPU time, only ¼ of the near well area is simulated, as indicated in blue in Figure C-1. Note that the flow in this part of the model domain is symmetrical to the flow in the other three parts. From the backbone ¼ of the diameter is simulated and for the laterals half the diameter.

The first layer of the model is reserved for representing the well above the reservoir. Only the grid block connected to the well is active. All other blocks are inactive. In this block a sink is located to allow the flow to leave the model. The grid block containing the sink is only connected to the reservoir via the grid blocks representing the well. The well representation will be explained further below.

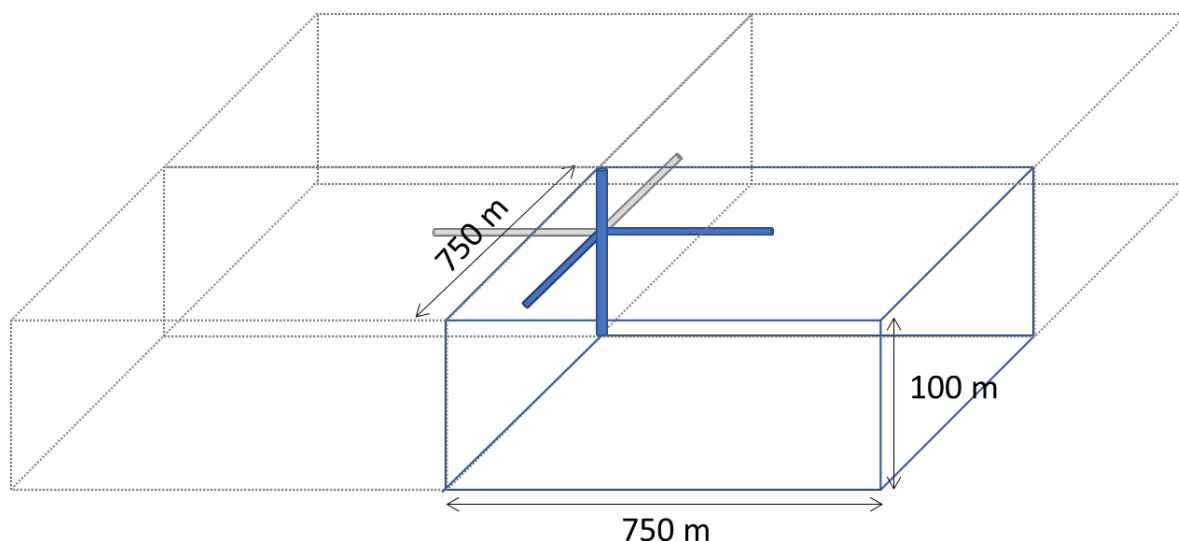


Figure C-1. Overview of the model setup with the radial well consisting of a vertical well with 4 perpendicular laterals.

*Representation of the well*

Both the well and laterals are simulated explicitly with grid blocks of 0.10 x 0.10 m. Thus, the diameter of the backbone is 0.20 m (four blocks of which 1 is simulated). The diameter of the laterals is 0.15 m (two blocks of 0.10 x 0.10 m of which 1 is simulated). In the top block of the well, a sink is defined to allow the flow to leave the model. The transmissibility between the sink and the block is taken very large to avoid pressure drop. The block containing the sink can be used to simulate well bore storage by increasing the block volume. For simulations with well bore storage, the pore volume of the well block is multiplied by 1000.

Permeability in the direction of the well needs to be set large to ensure low pressure drop in the well. For comparison with the results of AEM, which does not take into account pressure drop in the well, the pressure drop in the well is minimized. For that, the permeability in the

wells is set to 10 million D vertically and 1 million D horizontally. In the top part of the backbone, where the rate is 3600 sm<sup>3</sup>/d, the pressure drop is 56 Pa/m.

With smaller permeability in the wells, the model can represent pressure drop in the well. For a rate of 3600 sm<sup>3</sup>/d and a well diameter of 0.15 m, the pressure drop in the well is estimated as 635 Pa/m (assuming a roughness of 1 mm) [20]. To get a similar pressure drop in the simulation, permeability in the well should be set around 1 million D. For the laterals, the pressure drop is highly uncertain, because the rate is uncertain. If the pressure drop increases, the production/injection rate reduces. Also the increase in pressure drop is highly non-linear which cannot be represented because the Eclipse model can only account for Darcy type flow. For a lateral with a diameter of 0.04 m, a rate of 240 sm<sup>3</sup>/d and roughness of 5 mm, the pressure drop is 7300 Pa/m [20]. Similar values are achieved in the simulation model, by setting the permeability in the laterals to 10.000 D.

The boundary conditions of the model are set as follows:

- Lateral boundary condition: constant pressure at 758 m.
- Top and bottom boundary: no flow condition.

Grid size definition:

Different grid size distributions were tested in both horizontal and vertical direction, but this had little impact on the pressure drop and well test results.

Table C-1. Grid size used in the model

Horizontal direction		Vertical direction	
Number of cells	Cell size (m)	Number of cells	Cell size (m)
10	0.1**	6*	5
10	0.2	4	1.6
10	0.5	4	0.4
10	1	1	0.1**
10	2	5	0.6
10	4	4	1
10	8	12	5
10	16		
22	20		

\* For the first layer only the well block is active. All other grid blocks are set inactive.

\*\* This block is used to represent the well.

Reservoir and fluid properties are listed in Table 6-1. The fluid properties are consistent with a brine of 150.000 ppm at 75°C and 25 MPa. Both viscosity and compressibility are constant with pressure. The well flow rate used in the model is 900 sm<sup>3</sup>/d to take into account that only ¼ of the well and reservoir is simulated.

The results are sensitive to time stepping: due to the large contrasts in permeability, the time steps have to be large during the entire period to avoid numerical instability. At the start time stepping has to be small to capture the detailed pressure response near the well. Time step size starts at 0.864 s and grows to a maximum time step size of 110.6 s after 0.686 days.

Version 6/8/2020	Upscaling of RJD for incorporation in reservoir simulators	page 41 / 41
------------------	--	-----------------

**Appendix D. Peters et al. (2018) Modelling of multi-lateral well geometries for geothermal applications. *Advances in Geosciences*, 45: 209-215.**